Ecological Modelling 507 (2025) 111174

Contents lists available at ScienceDirect

Ecological Modelling

journal homepage: www.elsevier.com/locate/ecolmodel

Modelling forest-atmosphere exchanges of carbon and water using an improved hydro-biogeochemical model in subtropical and temperate monsoon climates

Wei Zhang [a], Xunhua Zheng [a,b], Siqi Li [a,*], Shenghui Han [a], Chunyan Liu [a,b], Zhisheng Yao [a,b], Rui Wang [a], Kai Wang [a], Xiao Chen [a,c], Guirui Yu [d,e], Zhi Chen [d,e,f], Jiabing Wu [g], Huimin Wang [d], Junhua Yan [h], Yong Li [i,*]

[a] State Key Laboratory of Atmospheric Environment and Extreme Meteorology, Institute of Atmospheric Physics, Chinese Academy of Sciences, Beijing, 100029, China
[b] College of Earth and Planetary Sciences, University of Chinese Academy of Sciences, Beijing, 100049, China
[c] Qilu Zhongke Institute of Carbon Neutrality, Jinan, 250100, China
[d] Key Laboratory of Ecosystem Network Observation and Modeling, Institute of Geographic Sciences and Natural Resources Research, Chinese Academy of Sciences, Beijing, 100101, China
[e] College of Resources and Environment, University of Chinese Academy of Sciences, Beijing, 100049, China
[f] Beijing Yanshan Earth Critical Zone National Research Station, University of Chinese Academy of Sciences, Beijing, 101408, China
[g] Institute of Applied Ecology, Chinese Academy of Sciences, Shenyang, 110016, China
[h] South China Botanical Garden, Chinese Academy of Sciences, Guangzhou, 510650, China
[i] State Key Laboratory of Earth System Numerical Modelling and Application, Institute of Atmospheric Physics, Chinese Academy of Sciences, Beijing, 100029, China

ARTICLE INFO

Keywords:
Forest ecosystem
Carbon fluxes
Process-based model
Sensitivity analysis
CNMM-DNDC

ABSTRACT

Forest-atmosphere carbon exchanges are crucial yet challenging to quantify accurately due to scaling uncertainties in site observations. Process-based models that mechanistically represent coupled carbon, nitrogen, and water cycling processes are theoretically capable of reducing uncertainties in forest carbon flux quantification, thereby improving predictions of multiple ecosystem variables relevant to achieving the United Nations Sustainable Development Goals (SDGs) by 2030. Thus, we enhanced the CNMM-DNDC model by developing a forest-specific growth module incorporating key processes (photosynthesis, allocation, respiration, mortality, litter decomposition) based on Biome-BGC formulations. Compared with the original model, evaluation against 8-year (2003–2010) eddy covariance data from three Asian forests showed significant improvements in the updated model. At daily and annual scales, normalized root mean square error decreased by 46% and 54% for gross primary productivity (GPP), and 65% and 37% for ecosystem respiration (ER), respectively, though net ecosystem carbon dioxide exchange (NEE) improvements were less pronounced due to error offsetting. Sensitivity analysis identified specific leaf area, fraction of leaf nitrogen in Rubisco and annual leaf and fine root turnover fraction as most influential eco-physiological parameters, with solar radiation, humidity and air temperature as dominant meteorological drivers. The model's ability to capture daily and inter-annual carbon flux variations demonstrates its potential for regional-to-global greenhouse gas assessments, while highlighting the need for component-specific validation to avoid error masking in net flux calculations.

1. Introduction

Forest ecosystems, covering nearly 40% of Earth's ice-free land surface (Waring and Running, 2007), provide critical ecological services beyond wood products. These include soil conservation, biodiversity maintenance, and regulation of global water and carbon cycles (Chiesi et al., 2007; Waring and Running, 2007). Forests significantly influence the global carbon cycle by regulating atmospheric carbon dioxide (CO_2) concentrations via photosynthesis. Remarkably, forest carbon sequestration offsets about 25% of annual anthropogenic CO_2 emissions from fossil fuel combustion and industry activities (Seidl et al., 2017; Cook-Patton et al., 2020; FAO, 2020). Therefore, accurate quantification

* Corresponding authors.
E-mail addresses: lisiqi@mail.iap.ac.cn (S. Li), yli@mail.iap.ac.cn (Y. Li).

https://doi.org/10.1016/j.ecolmodel.2025.111174
Received 14 April 2025; Received in revised form 7 May 2025; Accepted 7 May 2025
Available online 17 May 2025

of forest carbon fluxes, such as gross primary productivity (GPP) and ecosystem respiration (ER), is essential for understanding terrestrial carbon dynamics and climate change mitigation (Mao et al., 2016; Ren et al., 2022).

Various methods can be applied to estimate the carbon fluxes of forests, such as eddy-covariance measurements, satellite remote sensing, and numerical modelling. Numerical models are promising tools for integrating multi-source data and comprehensively representing vegetation-soil processes. These models can be categorized into three main types: statistical/regression models (Tatarinov and Cienciala, 2006; Raj et al., 2014), light use efficiency models (Running et al., 2004; Yuan et al., 2014) and process-based models. The latter, established based on fundamental principles of physics, chemistry, and biogeochemistry (Schulze et al., 2009; Hidy et al., 2012), treats the atmosphere-vegetation-soil-water continuum as an integrated dynamic system. These models enable estimation of terrestrial carbon budgets under multiple interacting environmental factors (Makela et al., 2000; Friedlingstein and Prentice, 2010; Mao et al., 2016).

Numerous process-based models (e.g., Biome-BGC, ORCHIDEE, LPJ) have been successfully implemented for simulating carbon cycling in natural/undisturbed forest ecosystems at regional to global scales (White et al., 2000; Sitch et al., 2003; Krinner et al., 2005). As managed ecosystems are playing essential roles in terrestrial carbon budget, more researches have focused on the managed ecosystems with significant anthropogenic activities recently, such as afforested forests and croplands (Cai et al., 2022; Ciais et al., 2013; Liu et al., 2022a; Mao et al., 2016; Miyauchi et al., 2019). Recent studies emphasize that carbon-climate interactions are fundamentally mediated by nitrogen availability and hydrology processes (Thornton et al., 2007; Piao et al., 2013). Incorporating carbon-nitrogen coupling and hydrological dynamics into process-based models has been shown to significantly alter simulated land-climate feedbacks (e.g., Churkina et al., 2009; Thomas et al., 2013). This recognition has driven substantial model developments, including the evolution of Biome-BGC into Biome-BGCMuSo, which integrates soil moisture dynamics, nitrogen cycling and vegetation managements modules for managed forests and croplands (Thornton et al., 2002; Bond-Lamberty et al., 2005; Tatarinov and Cienciala, 2006; Di Vittorio *et al.*, 2010; Hidy et al., 2016); extensions of natural ecosystem models (e.g., ORCHIDEE-STICS, LPJmL) to accurately represent interactions of carbon, nitrogen and water in agricultural systems (Gervois et al., 2004; Bondeau et al., 2007); development of specialized agroecosystem models (e.g., DNDC, WNMM, SPACSYS, WHCNS) addressing complex biogeochemical processes (Li et al., 1992; Li, 2007; Wu et al., 2007; Liang et al., 2016). For landscapes with complex topography (e.g., catchments, river basins), integrated hydro-biogeochemical models (e.g., LandscapeDNDC-CMF, SWAT-DayCent, CNMM-DNDC) have emerged as effective tools, capturing the tight coupling between biogeochemical and hydrological processes (Haas et al., 2012; Wu et al., 2016; Zhang et al., 2018).

The hydro-biogeochemical model of CNMM-DNDC was developed by integrating the Catchment Nutrient Management Model (CNMM) and the DeNitrification-DeComposition Model (DNDC). This coupled model has undergone several updates to improve its simulation of carbon, nitrogen, phosphorous and water cycling processes across multiple spatial scales, from site-level to regional applications. The model's distinctive features lies in its explicit representation of lateral water and nutrient transport through both surface and subsurface pathways, facilitated by grid-to-grid transfer algorithms that enable catchment-scale simulations. The CNMM-DNDC model has been applied in various climatic regions by simultaneously simulating ecosystem productivity, emissions of greenhouse gas and gaseous air pollutants, and nitrogen losses through leaching and stream discharge (Zhang et al., 2018; Zhang et al., 2021a; Zhang et al., 2021b; Li et al., 2022; Li et al., 2023). Model evaluation at a subtropical agro-forest catchment demonstrated its capability to simulate crop yields, soil organic carbon contents, emissions of methane, nitrous oxide, nitric oxide and ammonia, hydrological losses of nitrate and total nitrogen through surface runoff and stream flows, and sediment production (Zhang et al., 2018; Li et al., 2023). These validation results indicate that CNMM-DNDC can effectively represent key hydro-biogeochemical processes in terrestrial ecosystems.

While the CNMM-DNDC model has undergone substantial evaluation in agricultural systems, its performance in forest ecosystems requires further assessments due to the critical contribution of forests to global carbon budget (Seidl et al., 2017). The current version employs a vegetation growth module adapted from BIOME3 that treats plants as an entirety without accounting for biomass allocation among different tissues and/or organs. This simplified representation may introduce significant uncertainties in forest carbon and nitrogen simulations, as photosynthate allocation substantially influences these processes. We hypothesize that enhancing the vegetation growth module through improved representation of key physiological processes, including biomass allocation, respiration, and mortality, could substantially improve the model's performance across diverse forest ecosystems. Such improvements would address important limitations in the current modelling framework. First, as the CNMM-DNDC aimed at modelling or predicting of multiple ecosystem variables (including greenhouse gas fluxes, water cycling, and nutrient transport across spatial scales) concerned in the United Nations Sustainable Development Goals by 2030, deficiencies in forest ecosystem representation could constrain its utility for policy-relevant assessments. Second, an enhanced model version could provide new opportunities to investigate important climate change questions, such as permafrost thaw-induced soil carbon losses and their interactions with hydrological processes that have gained increasing scientific attention. These proposed developments would expand the model's applications to forest ecosystems while maintaining its existing strengths in simulating coupled biogeochemical and hydrological processes.

To validate this hypothesis, we conducted a comprehensive evaluation of both original and modified CNMM-DNDC by comparing their simulations of daily GPP, ER, net ecosystem CO_2 exchange (NEE) and evapotranspiration (ET) against multi-year continuous observations from three forest ecosystems under subtropical and temperate monsoon climates in eastern Asia. This study aims to (i) address critical gaps of simulation mechanisms in CNMM-DNDC by improving scientific processes of vegetation growth, (ii) systematically assess model performance across different forest types, and (iii) identify key ecophysiological parameters and input variables that significantly influence the simulated GPP and ER through multiple analytical approaches.

2. Materials and methods

2.1. Model description

2.1.1. Overview of CNMM-DNDC

The CNMM-DNDC model was initially developed by integrating the soil carbon and nitrogen transformation/transferring processes of the DNDC model (decomposition, nitrification, denitrification and fermentation) into the distributed hydrological framework of CNMM (Zhang et al., 2018). The original version maintained the phosphorous cycle and vegetation growth modules from CNMM (Li et al., 2017; Zhang et al., 2018), with subsequent updates enhancing its functionality and general applicability (Zhang et al., 2020; Zhang et al., 2021b; Li et al., 2022; Li et al., 2023). The model regards the atmosphere-vegetation-soil-water system as an integrated continuum, simulating coupled carbon, nitrogen and water cycles at catchment scales using the fundamental principles of physics, chemistry, and biogeochemistry. The data required for the simulation include land use type, stratified soil properties (organic carbon content, total nitrogen, clay fraction, bulk density, pH, etc.), meteorological forcing (hourly air temperature, precipitation, wind speed, solar radiation, etc.), biological parameters (plant functional type, nitrogen content, plant height, root depth, etc.), initial conditions (soil depth, soil temperature, soil moisture, annual amounts of dry and

wet nitrogen deposition etc.), management practices (start and end dates, methods and/or amounts of individual management practices including tillage, fertilization, irrigation and flooding for croplands), and boundary data (start date, period, time step, duration, depth of soil profile etc.). The model offers flexible spatial and temporal resolution options that users can customize according to data availability and research objectives.

The simulated soil profile could extend to depth of 4 m or more, though it does not currently incorporate groundwater circulation dynamics. The soil temperature is derived through energy balance and heat conductivity calculations, while soil moisture is determined by mass balance accounting for precipitation, irrigation, evapotranspiration, vertical and lateral water flows, and capillary rise from groundwater. At site-scale simulations, the model considers surface runoff while excluding subsurface lateral flow, with infiltration constrained by a user-defined maximum rate. Vertical water movement follows Darcy's law, while lateral flow routing employs a cell-by-cell kinematic approximation based on digital elevation model. Stream flow generation utilizes a cascade of linear channel reservoirs (Wigmosta et al., 1994). Biogeochemical processes are simulated using first-order kinetics for organic matter decomposition and Michaelis-Menten kinetics of dual substrates for nitrification and denitrification. The model employs an "anaerobic balloon" concept to accommodate concurrent oxidative and reductive reactions (Li, 2007). It specifically accounts for pH fluctuations following urea applications in both upland and paddy systems, as well as acidification processes in tea plantations. Detailed descriptions of biogeochemical processes are provided in Supplementary Tables S1−S3.

The current CNMM-DNDC model adopts vegetation growth algorithms adapted from the BIOME3 model (Haxeltine and Prentice, 1996a, b) to simulate plant growth across crops, forests, and grasslands. Among these processes, photosynthesis rate is calculated as functions of absorbed photosynthetically active radiation (APAR), temperature and atmospheric CO_2 concentration, following Farquhar et al. (1980) for C_3 species and Collatz et al. (1992) for C_4 plants. More explicitly, the net photosynthesis rate, i.e., net primary productivity, is calculated using a standard nonrectangular hyperbola formulation, which gives a gradual transition between two limiting rates describing the responses of photosynthesis to APAR and Rubisco abundance (Haxeltine and Prentice, 1996b). The plant growth simulation fails to account for two critical physiological processes which are biomass partitioning among different plant organs/tissues and plant mortality. Detailed descriptions of current vegetation growth implementation are available in Haxeltine and Prentice (1996a, b) and Zhang et al. (2018).

2.1.2. *Improvements of CNMM-DNDC*

This study developed an improved forest growth module for the CNMM-DNDC model by integrating key processes from the Biome-Bio Geochemical Cycles (Biome-BGC) model (White et al., 2000) to better simulate forest growth dynamics and associated carbon and water fluxes (Fig. 1). The module simulates stand-level processes on a per unit area basis, including photosynthesis, litter decomposition, photosynthate allocation, respiration, and mortality.

2.1.2.1. Carbon pools of forest ecosystems. The model's carbon pools comprise four major components: plant biomass, coarse woody debris, litter, and soil organic matter. The plant carbon pool is divided into subpools of leaves, fine roots, live stems (including both sapwood and heartwood), dead stems (primarily heartwood), live coarse roots, and dead coarse roots. Notably, the model does not explicitly differentiate between sapwood and heartwood components. Additionally, branches are treated as a constituent of live stems rather than as an independent plant carbon sub-pool. Upon mortality, dead stems and coarse roots initially enter the coarse woody debris pool before gradually fragmenting into litter pools. The litter pool consists of four chemically defined fractions: liable carbon, unshielded cellulose, shielded cellulose and lignin. The soil carbon pool excluding the litter carbon is initially inherited from the DNDC model, which includes the sub-pools of

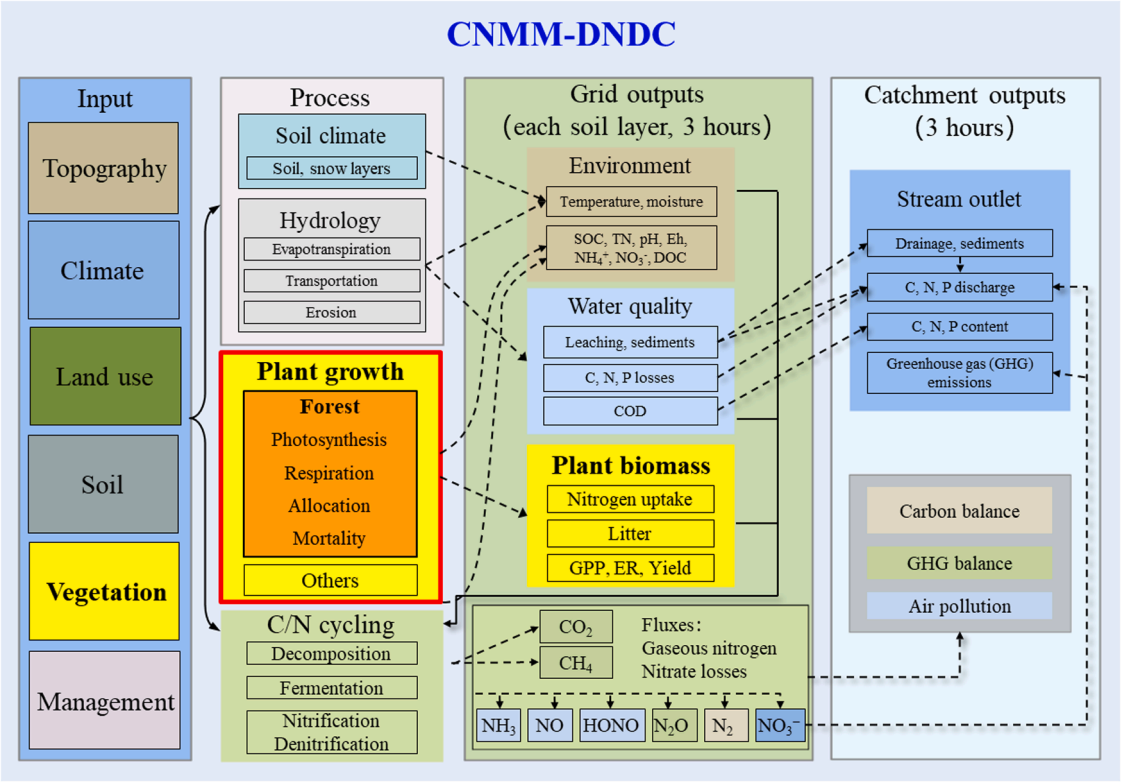

Fig. 1. The CNMM-DNDC framework incorporates a newly implemented module specifically designed to simulate forest growth processes.

microbes, humads and humus. The humads and humus defined in the DNDC indicate the liable humus and resistant humus with different decomposition rates.

2.1.2.2. Photosynthesis. Photosynthesis, as a fundamental process governing carbon accumulation in a forest ecosystem, is simulated through a two-leaf scheme that differentiates between sunlit and shaded leaves. This approach incorporates the biochemical model of photosynthesis while accounting for enzyme kinetics (Farquhar et al., 1980). The photosynthetic rate jointly depends on the amount of APAR, maintenance respiration (MR), CO_2 concentration gradient between leaf interior and atmosphere, leaf nitrogen content, the fraction of nitrogen in Rubisco, and temperature effects on enzyme kinetics.

The projected leaf area index of whole canopy ($PLAI_{total}$, in $m^2\ m^{-2}$) is calculated as the product of average specific leaf area (SLA, $m^2\ kg^{-1}$ C) based on carbon mass and leaf carbon content. The projected leaf area indexes for sun ($PLAI_{sun}$, $m^2\ m^{-2}$) and shade ($PLAI_{shade}$, $m^2\ m^{-2}$) leaves are calculated following Eqs. (1)−(2) (Jones, 1992).

$$PLAI_{sun} = 1 - e^{-PLAI_{total}} \quad (1)$$

$$PLAI_{shade} = PLAI_{total} - PLAI_{sun} \quad (2)$$

The APAR ($APAR_{total}$, $APAR_{sun}$, $APAR_{shade}$, W m^{-2}) is calculated based on the incoming shortwave radiation (Rads, in W m^{-2}), albedo (Alb, dimensionless), canopy light extinction coefficient (k, dimensionless), the $PLAI_{total}$, and the fraction of PAR in the incoming shortwave radiation (f_{par}, dimensionless) for the sun and shade leaves, respectively (Eqs. (3)−(5)).

$$APAR_{total} = f_{par}Rads(1.0 - Alb)\left(1.0 - e^{-kPLAI_{total}}\right) \quad (3)$$

$$APAR_{sun} = f_{par}kPLAI_{sun}Rads(1.0 - Alb) \quad (4)$$

$$APAR_{shade} = APAR_{total} - APAR_{sun} \quad (5)$$

The photosynthetic reaction rates are calculated through three distinct equations (Eqs. (6)-(8)), representing the biochemical process of sugar synthesis from CO_2 and H_2O using solar energy (Farquhar et al., 1980). Eq. (6) describes the photosynthetic rate limitation by either Rubisco activity (A_v, μmol $CO_2\ m^{-2}\ s^{-1}$) or electron transport (A_j, μmol $CO_2\ m^{-2}\ s^{-1}$), where C_a and C_i (Pa) denote atmospheric and intercellular CO_2 partial pressures, respectively. The C_a is derived from input atmospheric pressure (pa, Pa) and CO_2 concentration (C_{co_2}, μmol mol^{-1}) using Eq. (7). Following Eq. (8) (Nobel, 1991), stomatal conductance to CO_2 (g_{CO_2}, μmol $m^{-2}\ s^{-1}\ Pa^{-1}$) is calculated via incorporating water vapor conductance (g_{H_2O}, m s^{-1}), air temperature (T_{air}, °C), universal gas constant ($R = 8.3143$, m^3 Pa $mol^{-1}\ K^{-1}$), and the molecular weight ratio of water vapour to CO_2 (M). Both A_v and A_j in Eq. (6) are expressed on PLAI basis.

Total leaf conductance to water vapor (g_{H_2O}, m s^{-1}) is calculated by combining stomatal (g_s), boundary (g_{bl}), and cuticle (g_c) conductance in parallel for sun and shade leaves (Eqs. (9)−(12)). Maximum conductances of stomatal (g_{smax}), boundary (g_{blmax}), and cuticle (g_{cmax}) are user-defined eco-physiological parameters specified for different forest types in Table 1. A conductance correction factor (gcorr, dimemsionless) is calculated using air temperature (T_{air}, °C) and atmospheric pressure (pa, Pa) (Eq. (13)). While cuticle and boundary layer conductance are only

Table 1
Eco-physiological parameters used in the modified CNMM-DNDC model for forests in different humid monsoon climate.

Code	Parameters (unit)	CBM (Temperate)		QYZ (Subtropics)	DHM (South subtropics)	
p1	Forest type	DBT	ENT	ENT	EBT	ENT
p2	Start Julian date of new growth	121**	0*	0*	0*	0*
p3	End Julian date of litterfall	275**	0*	0*	0*	0*
p4	Transfer growth period as fraction of growing season (dimensionless)	0.2*	0.3*	0.3*	0.2*	0.3*
p5	Litterfall as fraction of growing season (dimensionless)	0.2*	0.3*	0.3*	0.2*	0.3*
p6	Annual leaf and fine roots turnover fraction (yr^{-1})	1.0*	0.32**	0.32**	0.5*	0.32**
p7	Annual live wood turnover fraction (yr^{-1})	0.7*	0.7*	0.7*	0.7*	0.7*
p8	Annual plant mortality fraction (yr^{-1})	0.0213**	0.009**	0.005*	0.005*	0.005*
p9	Annual fire mortality fraction (yr^{-1})	0.0**	0.0**	0.005*	0.0**	0.005*
p10	New fine root C: new leaf C (DIM)	0.9**	1.2**	1.0*	1.0*	1.0*
p11	New stem C: new leaf C (DIM)	2.4**	1.4**	2.2*	1.6**	2.2*
p12	New live wood C: new total wood C (dimensionless)	0.1*	0.379**	0.1*	0.22*	0.1*
p13	New coarse root C: new stem C (dimensionless)	0.23*	0.29**	0.3*	0.3*	0.3*
p14	Daily allocation to current growth (dimensionless)	0.5*	0.5*	0.5*	0.5*	0.5*
p15	C:N of leaves (dimensionless)	17.55**	34.3**	42*	42*	42*
p16	C:N of leaf litter (dimensionless)	41.1**	96.5**	93*	49*	93*
p17	C:N of fine roots (dimensionless)	47.4**	56.4**	42*	42*	42*
p18	C:N of live wood (dimensionless)	97.05**	97.4**	50*	50*	50*
p19	C:N of dead wood (dimensionless)	212**	398**	729*	300*	729*
p20−22	Leaf litter labile: cellulose: lignin (dimensionless)	53:22:25**	45:25:30**	32:44:24*	32:44:24*	32:44:24*
p23−25	Fine root labile: cellulose: lignin (dimensionless)	30:45:25*	34:44:22*	30:45:25*	30:45:25*	30:45:25*
p26−27	Dead wood cellulose: lignin (dimensionless)	76:24*	73:27**	76:24*	76:24*	76:24*
p28	Canopy light extinction coefficient (dimensionless)	0.58**	0.5*	0.5*	0.7*	0.5*
p29	All-side to projected leaf area ratio (dimensionless)	2.0*	2.6*	2.6*	2.0*	2.6*
p30	Canopy average specific leaf area (SLA) ($m^2\ kg^{-1}$ C)	54.2**	16.4**	12.0*	12.0*	12.0*
p31	Shaded SLA: sunlit SLA (dimensionless)	2.0*	2.0*	2.0*	2.0*	2.0*
p32	Fraction of leaf N in Rubisco (dimensionless)	0.075# (0.04–0.16)	0.10# (0.04–0.16)	0.055# (0.02–0.08)	0.03# (0.03–0.12)	0.03# (0.02–0.08)
p33	Maximum stomatal conductance (m s^{-1})	0.0065**	0.006**	0.003*	0.005*	0.003*
p34	Cuticular conductance (m s^{-1})	0.00001**	0.000006**	0.00001*	0.00001*	0.00001*
p35	Boundary layer conductance (m s^{-1})	0.01*	0.09**	0.08*	0.01*	0.08*
p36	Vapor pressure deficit: start of conductance reduction (Pa)	1100**	610**	930*	1800*	930*
p37	Vapor pressure deficit: complete conductance reduction (Pa)	3600**	3100**	4100*	4100*	4100*

CBM is the Changbai Mountains site (in Jilin Province) with a mixed forest of deciduous broadleaf trees (DBT) and evergreen needleleaf trees (ENT) subjected to a humid temperate monsoon climate. DHM is the Dinghu Mountains site (in Guangdong Province) with a mixed forest of evergreen broadleaf trees (EBT) and ENT subject to a humid southern subtropical monsoon climate. The superscripts of *,** and # indicate that the values of parameters are obtained from the model default values, other studies and model calibration, respectively. The values in the parenthesis indicate the upper and lower boundaries of the calibrated parameter.

scaled by gcorr, stomatal conductance incorporates additional multipliers (Eq. (14); f) of photosynthetic photon flux density (f_{PPFD}), soil water potential (f_{SM}), minimum temperature (f_{Tair}), and vapour pressure deficit (f_{VPD}). The f_{PPFD} calculation considers photosynthetic photon flux density (PPFD, μmol m^{-2} s^{-1}), projected leaf area index of whole canopy (PLAI, m^2 m^{-2}) and the PPFD threshold for 50% stomatal closure (75 μmol m^{-2} s^{-1}), which is computed separately for sun and shade leaves (Eq. (15)). Other multipliers are calculated based on current, maximum and minimum values of respective variables for all leaves.

$$A_{\text{v or j}} = g_{CO_2}\left(C_a - C_i\right) \tag{6}$$

$$C_a = 10^{-6} C_{co_2} pa \tag{7}$$

$$g_{CO_2} = \frac{10^6 g_{H_2O}}{M \times R(T_{air} + 273.15)} \tag{8}$$

$$g_{H_2O} = \frac{g_{bl}(g_s + g_c)}{g_{bl} + g_s + g_c} \tag{9}$$

$$g_s = g_{smax} gcorr f \tag{10}$$

$$g_{bl} = g_{blmax}\ gcorr \tag{11}$$

$$g_c = g_{cmax} gcorr \tag{12}$$

$$gcorr = \left[\frac{(T_{air} + 273.15)}{293.15}\right]^{1.75} \frac{101300}{pa} \tag{13}$$

$$f = f_{PPFD} f_{SM} f_{Tair} f_{VPD} \tag{14}$$

$$f_{PPFD} = \frac{PPFD/PLAI}{75 + PPFD/PLAI} \tag{15}$$

The A_v is calculated through Eqs. (16)-(23). In Eq. (17), maximum carboxylation rate (V_{max}, μmol CO_2 m^{-2} s^{-1}) is a function of leaf nitrogen content per unit area (N_{leaf}, kg N m^{-2}), the fraction of leaf nitrogen in Rubisco as an input parameter (FLNR, kg N kg^{-1} leaf N), the weight proportion of Rubisco relative to its nitrogen content (WP = 7.16, kg Rub kg^{-1} Rubisco N) (Fasman, 1976) and activity of Rubisco (AC, μmol CO_2 kg^{-1} Rub s^{-1}). Notably, co-limitation of photosynthetic capacities by leaf phosphorous has not been considered. Using Eq. (18), nitrogen concentration (N_{leaf}) in sun and shade leaves are calculated based on the input parameters of leaf carbon to nitrogen ratio (r_{cnl}, dimensionless) and specific leaf area (SLA, m^2 kg^{-1} C). In Eq. (19), the AC is temperature adjusted from its standard value at 25 °C ($AC_{25} = 6 \times 10^4$ μmol CO_2 kg^{-1} Rub s^{-1}) using a temperature sensitivity coefficient (Q_{10AC}, dimensionless) of 2.4 (Woodrow and Berry 1988). The CO_2 compensation point (γ, Pa), excluding leaf maintenance respiration (MR_{leaf}, μmol CO_2 m^{-2} s^{-1}), depends on atmospheric oxygen partial pressure (C_{O_2}, assumed as 21% of air pressure, Pa) and temperature-adjusted kinetic constants for Rubisco carboxylation (K_c, Pa) and oxygenation (K_o, Pa), with base values of 40.4 Pa and 24800 Pa at 25 °C, respectively (Eqs. (20)-(23)). The temperature sensitivity coefficients (Q_{10}) for these constants are 2.1 (K_c) and 1.2 (K_o) (Woodrow and Berry 1988). All calculations of MR_{leaf} in Eq. (16) are expressed on PLAI basis (refer to the section of 2.1.2.5).

$$A_v = \frac{V_{max}(C_i - \gamma)}{C_i + K_c\left(1 + \frac{C_{O_2}}{K_o}\right)} - MR_{leaf} \tag{16}$$

$$V_{max} = WP N_{leaf} FLNR \times AC \tag{17}$$

$$N_{leaf} = \frac{1}{r_{cnl} SLA} \tag{18}$$

$$AC = \begin{cases} \dfrac{1.8 AC_{25} Q_{10AC}^{\left(\frac{T_{air}-15}{10}\right)}}{Q_{10AC}} & T_{air} \le 15\ ^\circ C \\ AC_{25} Q_{10AC}^{\left(\frac{T_{air}-25}{10}\right)} & T_{air} > 15\ ^\circ C \end{cases} \tag{19}$$

$$\gamma = 0.5 K_c \frac{C_{O_2}}{K_0} \tag{20}$$

$$C_{O_2} = 0.21 Air \tag{21}$$

$$K_c = \begin{cases} \dfrac{1.8 K_{c25} Q_{10K_c}^{\left(\frac{T_{air}-15}{10}\right)}}{Q_{10K_c}} & T_{air} \le 15\ ^\circ C \\ K_{c25} Q_{10K_c}^{\left(\frac{T_{air}-25}{10}\right)} & T_{air} > 15\ ^\circ C \end{cases} \tag{22}$$

$$K_o = K_{o25} Q_{10K_o}^{\left(\frac{T_{air}-25}{10}\right)} \tag{23}$$

The A_j is calculated using Eqs. (24)-(27). In the Eq. (25) (de Pury and Farquhar, 1997), the electron transport rate per unit leaf area (J, μmol CO_2 m^{-2} s^{-1}) is determined by the maximum potential electron transport rate (J_{max}, μmol CO_2 m^{-2} s^{-1}), curvature parameter ($\theta_1 = 0.7$) describing the light response curve, and PAR effectively absorbed by photosynthesis per unit leaf area (I_e, μmol CO_2 m^{-2} s^{-1}). The I_e is derived from Eq. (26), based on total absorbed PAR per unit leaf area (I, μmol CO_2 m^{-2} s^{-1}), a spectral correction factor ($f_{sc} = 0.15$), and the quantum requirement for electron transport (ppe, mol mol^{-1}). The I is calculated by converting APAR to photon flux density using a conversion factor (EPAR) of 4.55 μmol CO_2 m^{-2} s^{-1} per W m^{-2}, then normalizing by PLAI for both sun and shade leaves (Eq. (27)). The values of ppe are 2.6 and 3.5 for C_3 and C_4 plant, respectively.

$$A_j = \frac{J(C_i - \gamma)}{4.5C_i + 10.5\gamma} - MR_{leaf} \tag{24}$$

$$\theta_1 J^2 - (I_e + J_{max})J + I_e J_{max} = 0 \tag{25}$$

$$I_e = I\frac{(1 - f_{sc})}{ppe} \tag{26}$$

$$I = EPAR\frac{APAR_{sun/shade}}{PLAI_{sun/shade}} \tag{27}$$

Eqs. (6) and (16) are solved for C_i, which in turn is introduced into Eq. (24) to solve A_j. The smaller value between the A_v and A_j solutions is accepted as the rate of photosynthesis on the PLAI basis.

2.1.2.3. Litter decomposition. The model simulates carbon and nitrogen cycling through distinct organic matter pools with specific transfer pathways. Dead leaves and fine roots contribute carbon and nitrogen directly to four litter compartments according to specified allocation ratios, while nitrogen resorption prior to leaf senescence is regulated by the ratio of carbon to nitrogen of leaf litter. Live stems and coarse roots transition to dead pools through daily turnover processes controlled by annual maximum live woody mass and specified live wood turnover rate. These dead stems and coarse roots first enter the coarse woody debris pool, and then progressively fragment into finer litter fractions at a potential rate (R_{frag_CWD}, d^{-1}) influenced by soil moisture and temperature (Eqs. (28)-(29)). The fragmented coarse woody debris is distributed among specific litter pools based on the relative proportions of labile, cellulose, or lignin carbon fractions, as user-defined parameters. The litter pools then decompose and enter into soil organic matter

pools. The decomposition of shielded cellulose, liable carbon, unshielded cellulose and lignin to unshielded cellulose, liable microbe, liable humads and resistant humads, as well as the heterotrophic respiration and nitrogen immobilization by microbes during these processes, are considered in the model. Following Eq. (30) (White et al., 2000), potential nitrogen immobilization rates (N_{immo_p}, kg N m^{-2} $(3h)^{-1}$) during decomposition are calculated based on carbon decomposition potential (C_{decom_p}, kg C m^{-2} $(3h)^{-1}$) under potential decomposed rate (R_{dec_p}, d^{-1}), fractions of heterotrophic respiration (f_{HR}, dimensionless), and C:N ratio of litter (R_{litCN}, dimensionless) and soil organic matter (R_{soilCN}, dimensionless). The fractions and maximum rates related to decomposition processes, as well as heterotrophic respiration, are all defined as constants (Table S4). The decomposition rates are also adjusted by soil temperature (t_adjust; T_{soil}, °C) and moisture (w_adjust) as showed in Eqs. (28)-(29), with the calculated soil water potential under saturation. The minimum soil water potential ($Min_{potential}$) was set as −10 Mpa. The model maintains strict nitrogen mass balance by competitively allocating soil mineral nitrogen between plant growth and decomposition demands, automatically downregulating decomposition rates under nitrogen limitation conditions as specified in section of 2.1.2.4.

$$t\_adjust = \begin{cases} e^{4.344692 - \frac{1}{(T_{soil}+273.15) - 227.13}} & T_{air} \geq -10°C \\ 0 & T_{air} < -10°C \end{cases} \quad (28)$$

$$w\_adjust = \begin{cases} \frac{\ln\left(\frac{Min_{potential}}{SM_{potential}}\right)}{\ln\left(\frac{Min_{potential}}{Sat_{potential}}\right)} & SM_{potential} > Sat_{potential} \\ 1.0 & SM_{potential} > Sat_{potential} \\ 0.0 & SM_{potential} < Min_{potential} \end{cases} \quad (29)$$

$$N_{immo\_p} = C_{decom\_p}\frac{1 - f_{HR} - \frac{R_{soilCN}}{R_{litCN}}}{R_{soilCN}} \quad (30)$$

2.1.2.4. Allocation. The model calculates carbon allocation patterns and nitrogen competition processes based on two key variables: (1) the potential assimilated carbon from photosynthesis (C_{assi_p}, kg C m^{-2} $(3h)^{-1}$) and (2) the potential nitrogen demand during organic matter decomposition (N_{immo_p}, kg N m^{-2} $3h^{-1}$). These calculations determine the partitioning of newly fixed carbon among plant tissues while resolving the competitive nitrogen demands between plant uptake and microbial immobilization during litter decay.

The model determines assimilated carbon (C_{assi_p}, kg C m^{-2} $(3h)^{-1}$) available to allocate as the difference between gross primary productivity (GPP, kg C m^{-2} $(3h)^{-1}$) and MR (kg C m^{-2} $(3h)^{-1}$) across all live tissues, with negative values indicating carbon pool deficits. This carbon pool deficit must be repaid within one year through prioritized allocation. Carbon allocation follows strict hierarchical rules where new leaf production takes precedence over stem growth under stress conditions (Waring and Pitman, 1985; Waring and Running, 2007). The carbon cost for per unit of leaf growth ($C_{allometry}$, dimensionless), which is the carbon allometry, incorporates both growth respiration cost (f_{GR}, dimensionless, 30% of new tissue carbon) and user-defined structural allocation rates of new fine root carbon to new leaf carbon (r_{frtol}, dimensionless), new stem carbon to new leaf carbon (r_{stol}, dimensionless), new live wood carbon to new total wood carbon (r_{lwtow}, dimensionless), and new coarse root carbon to new stem carbon (r_{crtos}, dimensionless) (Eq. (31)). Associated nitrogen requirements by per unit of leaf growth ($N_{allometry}$, dimensionless) are derived from tissue-specific C:N ratios of leaves (R_{lCN}, dimensionless), fine roots (R_{frCN}, dimensionless), live woods (R_{lwCN}, dimensionless) and dead woods (R_{dwCN}, dimensionless) (Eq. (32)). Total nitrogen demand (N_{demand}, kg N m^{-2} $(3h)^{-1}$) integrates competing requirements for plant growth (N_{assi_p}, kg N m^{-2} $(3h)^{-1}$) and potential microbial immobilization during decomposition (N_{immo_p}, kg N m^{-2} $(3h)^{-1}$), with the former calculated from potential assimilated carbon (C_{assi_p}, kg C m^{-2} $(3h)^{-1}$), carbon allometry ($C_{allometry}$, dimensionless) and nitrogen allometry ($N_{allometry}$, dimensionless) (Eq. (33)).

$$C_{allometry} = (1 + f_{GR})[1 + r_{frtol} + r_{stol}(1 + r_{crtos})] \quad (31)$$

$$N_{allometry} = \frac{1}{R_{lCN}} + \frac{r_{frtol}}{R_{frCN}} + \frac{r_{stol}r_{lwtow}(1 + r_{crtos})}{R_{lwCN}} + \frac{r_{stol}(1 - r_{lwtow})(1 + r_{crtos})}{R_{dwCN}} \quad (32)$$

$$N_{assi\_p} = C_{assi\_p}\frac{N_{allometry}}{C_{allometry}} \quad (33)$$

When soil mineral nitrogen (N_{soil}, kg N m^{-2} $(3h)^{-1}$) suffices to meet total nitrogen demand, both plant allocation and litter decomposition proceed at potential rates. Plant nitrogen uptake prioritizes retranslocated nitrogen before utilizing soil mineral nitrogen, while decomposition relies solely on soil mineral nitrogen. Under nitrogen limitation ($N_{soil} < N_{demand}$), decomposition is reduced by a scaling factor (FPI) derived from the ratio N_{immo_p} to N_{demand} (Eq. (34)). Plant nitrogen allocation maintains priority, with proportional reductions occurring only when nitrogen pools are insufficient to meet demand (Wang et al., 2009). This framework ensures nitrogen competition between plants and decomposers while maintaining mass balance.

$$FPI = \frac{N_{soil}\frac{N_{immo\_p}}{N_{demand}}}{N_{immo\_p}} \quad (34)$$

2.1.2.5. Respiration. Maintenance respiration (MR, kg C m^{-2} $(3h)^{-1}$) is calculated separately for leaves, fine roots, live stems, and live coarse roots based on nitrogen content of tissues (N, kg N m^{-2}), temperature sensitivity (Q_{10} = 2.0) and $T_{air/soil}$, using a conversion factor (8.0) to translate daily rates to 3-hour intervals (Eq. (35)). Following Ryan (1991), MR responds linearly to nitrogen concentration across all tissues at 0.218 kg C d^{-1} kg^{-1} N. For leaves specifically, maintenance respiration (MR_{leaf}, μmol CO_2 m^{-2} s^{-1}) is computed separately for sun and shade leaves on a PLAI basis, incorporating leaf nitrogen concentration on the PLAI basis (N_{leaf}, kg N m^{-2}), Q_{10}, T_{air} and the molar mass of carbon (M_{CO_2} = 12 g mol^{-1}), with a conversion factor (86400) adjusting daily rates to seconds (Eq. (36)).

$$MR = \frac{0.218NQ_{10}^{\frac{T_{air/soil}-20}{10}}}{8.0} \quad (35)$$

$$MR_{leaf} = \frac{0.218N_{leaf}Q_{10}^{\frac{T_{air}-20}{10}}}{86400 \times 10^{-9}M_{CO_2}} \quad (36)$$

Growth respiration (GR, kg C m^{-2} $(3h)^{-1}$) is calculated separately for leaves, fine roots, live stems, and live coarse roots by allocating a portion

of each organ's carbon to its respective GR pool. This stored GR pool is then either fully or partially utilized for growth in the subsequent year governed by two key parameters. One is the fraction of carbon respired during growth ($g_1 = 0.3$). And the other is the proportion of growth respiration to release at fixation ($g_2 = 1.0$). The carbon pools of each plant organ are determined within the allocation module.

2.1.2.6. Mortality. The model calculates mortality for all plant organs using user-defined rates, with dead tissues transferring to coarse woody debris and litters pools at each time step. Additionally, fire-induced mortality can be simulated through user-specified parameters, accounting for associated carbon and nitrogen losses to the atmosphere through combustion processes.

2.2. Description of observed data

The observed data for model evaluation were obtained from ChinaFLUX (Chinese Terrestrial Ecosystem Flux Observation and Research Network), which has conducted continuous measurements of carbon and water fluxes in typical East Asian forest using open-path eddy covariance techniques since its establishment in 2002 (http://www.chinaflux.org/enn/index.aspx). The study utilized data from three representative sites: (1) a temperate mixed forest (evergreen needleleaf and deciduous broadleaf) at Changbai Mountain (CBM, 42°24′09″N, 128°05′45″E, 738 m a.s.l.); (2) a subtropical artificial evergreen coniferous forest at Qianyanzhou (QYZ, 26°44′29″N, 115°03′29″E, 102 m a.s.l.); and (3) a subtropical evergreen mixed forest (broadleaf and needleleaf) at Dinghu Mountain (DHM, 23°10′25″N, 112°32′04″E, 300 m a.s.l.) (Yu et al., 2008, 2013; Zhang et al., 2019a). Continuous observational carbon and water fluxes (2003−2010), including daily GPP, ER, NEE and ET, were collected in these undisturbed forest reserves for model calibration and evaluation, along with complete hourly meteorological records (air temperature, precipitation, radiation, wind speed and humidity) serving as model inputs. Additional site information is detailed in Text S1 and Table S5.

2.3. Model simulation

The modified CNMM-DNDC was calibrated (2003−2007) and evaluated (2008−2010) using carbon and water flux data from three forest sites. Required 3-hourly climate inputs (T_{air}, precipitation (Prec), wind speed (Wind), solar radiation (Rad), and relative humidity (Hum)) and soil properties (clay fraction, organic matter (SOM), total nitrogen, pH and bulk density (BD)) were obtained from the National Ecosystem Science Data Center (NESDC; https://www.nesdc.org.cn/), with nitrogen deposition rates derived from annual dry and wet nitrogen deposition data (Jia et al., 2019; 2021). Climate data out of the observational period were supplemented from the China meteorological forcing dataset (1979–2018) (https://data.tpdc.ac.cn), while additional soil hydraulic parameters, including field capacity, wilting point and saturated hydrological conductivity, were estimated using pedo-transfer functions (Li et al., 2019).

Forest composition was simplified as homogeneous mixtures: CBM as deciduous broadleaf (DBT)/evergreen needleleaf (1:1), DHM as evergreen broadleaf (EBT)/needleleaf (1:1), and QYZ as pure evergreen needleleaf (ENT) forest. Key vegetation parameters, such as forest type, carbon contents of leaf and stem, were derived from field observations (NESDC) and literatures (Li, 2018; Li, 2019; Fang, 2022), with remaining eco-physiological parameters set as default values (Table 1). The parameter of fraction of leaf nitrogen in Rubisco (p32) was calibrated by minimizing normalized root mean square error (NRMSE) between observed and simulated carbon and water fluxes (2003–2007), with bounds set at 0.5–2 times of default values. Nitrogen fixation was fixed at 0.0004 kg m^{-2} y^{-1} (Biome-BGC default) (Fang, 2022).

The soil profile (0−1.5 m in depth), with the last layer set as rock, was divided into 16 layers and the layer thicknesses were 0.05, 0.1 and 0.5 cm for depths of 0–0.5, 0.5–1 and 1–1.5 m, respectively, according to previous studies (Guan et al., 2006; Zeng et al., 2008; Zhou et al., 2013). The model simulations were conducted at 3-hour intervals for each forest site. Initial soil carbon and nitrogen pools were set using observational data, while the forest initial state was determined by observed leaf and stem carbon contents along with allocation rates among plant organs, which was not the model's native dynamics (Table S5; Thornton and Rosenbloom, 2005). To achieve stable carbon and nitrogen cycling (Zhang et al., 2015a), which requires spin-up for at least 10 years (Palosuo et al., 2012), we pre-ran simulations for 13 years until soil organic carbon changes (including microbes, humads and humus) stabilized below 50 kg C ha^{-1} yr^{-1}. Spin-up climate data came from the China meteorological forcing dataset (1979–2018) (https://data.tpdc.ac.cn). Model simulation error (ε_s), representing deviations between simulations and observations, was decomposed into structural (ε_{model}) and input-related (ε_{input}) uncertainties following Zhang et al. (2020), with calculation methods described in Text S2.

2.4. Sensitivity analysis

We conducted one-at-a-time (OAT) sensitivity analysis to evaluate how newly introduced parameters and key input variables affect simulated GPP and ER in the modified CNMM-DNDC. Using 2008–2010 evaluation period simulations as baseline, we examined: (1) eco-physiological parameters from the new forest growth module and Q_{10} of maintenance respiration (default = 2.0); (2) meteorological inputs (3-hourly T_{air}, Rad, Wind, Hum and Prec) and soil properties (clay fraction, pH, SOM and BD). Parameters were perturbed by ± 10%, ± 15% and ± 20% (White et al., 2000), except for T_{air} (± 1 °C increments within ± 3 °C), BD (site-specific ranges with 0.04 intervals), and pH (site-specific ranges with 0.2 intervals). Sensitivity was quantified using a sensitivity index (I, %) calculated in Eq. (37) (Majkowski et al., 1981), with NEE excluded as it derives from the difference between ER and GPP.

$$I = \frac{100\sum_{i=1}^{n}(|M_i - M_{baseline}|)}{n M_{baseline}} \quad (37)$$

In Eq. (37), we calculates the sensitivity index (I) by comparing simulated annual GPP or ER values under parameter/input variations (M_i) against baseline values ($M_{baseline}$), where $n = 6$ represents the total number of perturbations tested for each variable. For each forest type, we report the three-year mean and standard deviation of I values, quantifying the sensitivity of carbon fluxes to parameter/input variations.

To complement the OAT approach, we implemented the Morris global sensitivity analysis to account for parameter interactions. This method evaluates parameter sensitivity through elementary effects (d_i, i ∈ (1, 2, …, k)) calculated along multiple trajectories in a normalized parameter space (0–1 range). For k parameters discretized into p levels, each trajectory involves (k + 1) nodes generated by systematically perturbing one parameter at a time while holding others constant. From m such trajectories, we computed three statistics of d (Eq. (38)) for each parameter: mean elementary effect (μ, Eq. (39)), absolute average value (μ^*, Eq. (40)) and standard deviation (σ, Eq. (41)). Following Campolongo et al. (2007), we prioritized for parameter ranking due to its robustness for non-monotonic systems (Morris, 1991; Saltelli et al., 2008). Further details regarding the Morris approach are provided in Text S3.

$$d_{ij} = \frac{f(X_1, X_2, \ldots, X_{i-1}, X_i + \Delta, \ldots, X_k) - f(X_1, X_2, \ldots, X_k)}{\Delta} \quad (38)$$

$$\mu_i = \frac{1}{m}\sum_{j=1}^{m} d_{ij} \quad (39)$$

$$\mu_i^* = \frac{1}{m}\sum_{j=1}^{m}|d_{ij}| \quad (40)$$

$$\sigma_i = \sqrt{\frac{1}{m-1}\sum_{j=1}^{m}(d_{ij} - \mu_i)^2} \quad (41)$$

In Eq. (38), d_{ij} represents the elementary effect for the jth trajectory of the ith parameter, where, $i \in (1, 2, \ldots, k)$ and $j \in (1, 2, \ldots, m)$; X_i is the ith input parameter; and $f(X)$ denotes annual output values during 2008–2010. Our analysis employed $k = 40$ parameters and $m = 50$ trajectories across all sites. A high value of μ^* indicates high sensitivity of the parameter, while $\sigma > 0$ indicates parameter interactions, with $\sigma = 0$ signifying independent effects.

2.5. Statistics and analysis

Three statistical criteria were used to evaluate model performance (Eqs. (42)-(44)): (1) normalized root mean square error (NRMSE), where values approaching 0 indicate better agreement; (2) Nash–Sutcliffe efficiency (NSE, ranging from minus infinity to 1), with 1 representing perfect simulation and values between 0–1 denoting acceptable performance; and (3) determination coefficient (R^2) and slope of a significant linear zero-intercept regression (ZIR), where simultaneous proximity to 1 for both parameters indicates superior model performance (Nash and Sutcliffe, 1970; Willmott and Matsuurra, 2005; Moriasi et al., 2007; Congreves et al., 2016; Dubache et al., 2019). The absolute divergence of the slope from 1 represents the average bias of simulations from observations (Zhang et al., 2019b).

$$\mathrm{NRMSE} = \frac{1}{|\overline{O}|}\sqrt{\frac{\sum_{i=1}^{n}(S_i - O_i)^2}{n}} \quad (42)$$

$$\mathrm{NSE} = 1 - \frac{\sum_{i=1}^{n}(S_i - O_i)^2}{\sum_{i=1}^{n}(O_i - \overline{O})^2} \quad (43)$$

$$R^2 = 1 - \frac{\sum_{i=1}^{n}(O_i - \widehat{O}_i)^2}{\sum_{i=1}^{n}(O_i - \overline{O})^2} \quad (44)$$

In Eqs. (42)-(44), i ($i = 1, 2, \ldots, n$) represents each paired comparison among model simulations (S), observations (O) and predictions ($\widehat{O}$) by linear regression, respectively, where n indicates the total number of data pairs (see Tables S6-S7) and $\overline{O}$ denotes the mean observed value.

Taylor diagrams were employed to comprehensively assess model performance by simultaneously displaying three key statistical criteria: (1) correlation coefficients (r) between simulated and observed daily fluxes, (2) centred root mean square difference (RMSD), and (3) standard deviations (SD) of both observations (reference) and simulations. In these diagrams, normalized SD (NSD) equals 1 for observations, while simulation NSD represents the ratio of simulated to observed variability. Optimal model performance is indicated when simulation points approach the reference point ($r = 1$, NSD = 1, RMSD = 0), with improved versions showing closer proximity to this ideal position than the original model. Separate diagrams were generated for each carbon/water flux variable (GPP, ER, NEE, ET) across all three study sites.

All statistical analysis and graphical comparisons were performed using SPSS Statistics 19.0 (SPSS Inc., Chicago, USA), Origin 8.0

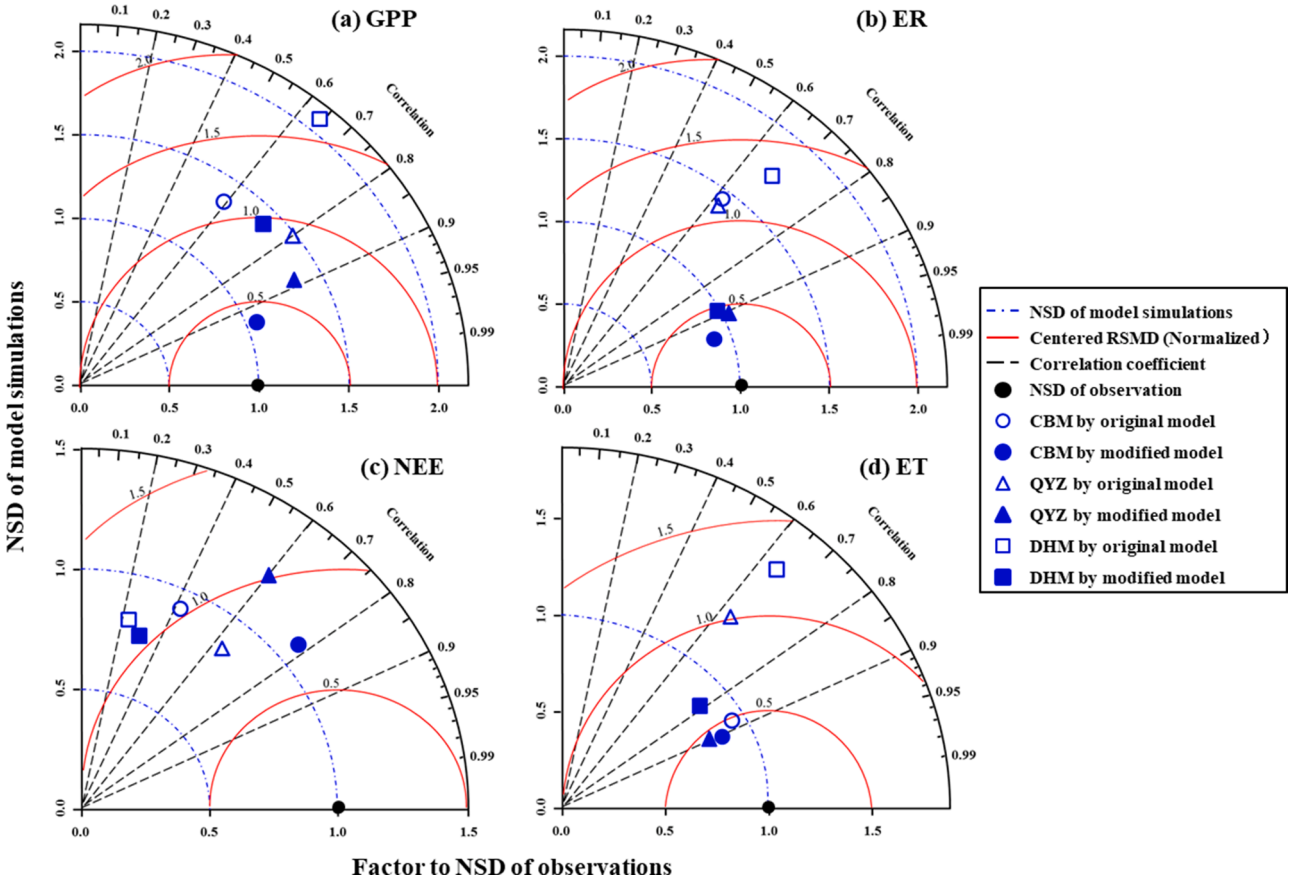

Fig. 2. Performance of original (empty grey symbols) and modified (solid blue symbols) model versions compared to observations (black solid points) at each forest site in evaluation years (2008–2010). Statistics shown in the Taylor diagrams are for daily simulated and observed carbon fluxes of gross primary productivity (GPP), ecosystem respiration (ER) and net ecosystem-atmosphere exchange of carbon dioxide (NEE), and water vapour fluxes of evapotranspiration (ET). The full site names of CBM, QYZ, and DHM are referred to the footnotes of Table 1.

(OriginLab, Northampton, MA, USA), and R software packages. The source code, executable program of the improved model, and corresponding input data are publicly available through Zhang *et al.* (2024).

3. Results

3.1. Model performances in simulating carbon and water fluxes

The three forest sites exhibited distinct seasonal GPP patterns that correlated with air temperature dynamics, though the DHM site located in the south margin of subtropical region showed weaker seasonality than the other sites. While the original model produced premature seasonal peaks at CBM, larger inter-day fluctuations at QYZ, and overestimated peak fluxes at both CBM and DHM sites (Figs. S1a, S2a and S3a), the modified version demonstrated marked improvements. Evaluation criteria for the modified model showed NRMSE (0.33–0.41), NSE (0.08–0.89), R^2 (0.18–0.90), and regression slopes (0.85–0.94) (Table S6), with particularly strong performance at CBM (NSE≈0.88, R^2≈0.89, slope≈0.94). Taylor diagrams (Fig. 2a) also confirmed the modified model's superior performance across all sites. Notably, substantial overestimations of original model in growing-season at CBM and DHM resulted in unacceptable statistics (Table S6). The modified model not only better captured daily GPP dynamics but also more accurately represented inter-annual variations, maintaining NSE > 0.60 during both calibration and validation periods (Figs. 3a–c, Table S7).

Observed daily ER exhibited similar seasonal patterns to GPP but with approximately double the peak values at CBM compared to DHM. While the original model showed premature seasonal peaks at CBM, excessive variability at QYZ, and overestimated seasonal fluxes at both CBM and DHM sites, the modified model demonstrated significantly improved performance. Evaluation criteria for the modified model showed NRMSE (0.18–0.27), NSE (0.62–0.93), R^2 (0.68–0.93), and regression slopes (0.92–1.05) (Table S6), with Taylor diagrams confirming superior correlation coefficients across all sites (Fig. 2b). Annual ER simulations showed particular strong improvement (NSE = 0.56 v.s. 0.05 for the original model; Table S7), indicating the modified model's enhanced capability to simulate combined autotrophic and heterotrophic respiration across temperate to subtropical monsoon forests in East Asia (Figs. 3d−f).

Daily NEE observations revealed pronounced seasonality at the temperate CBM site but weaker patterns at the subtropical QYZ and DHM sites (Figs. S1c, S2c and S3c). The modified model showed

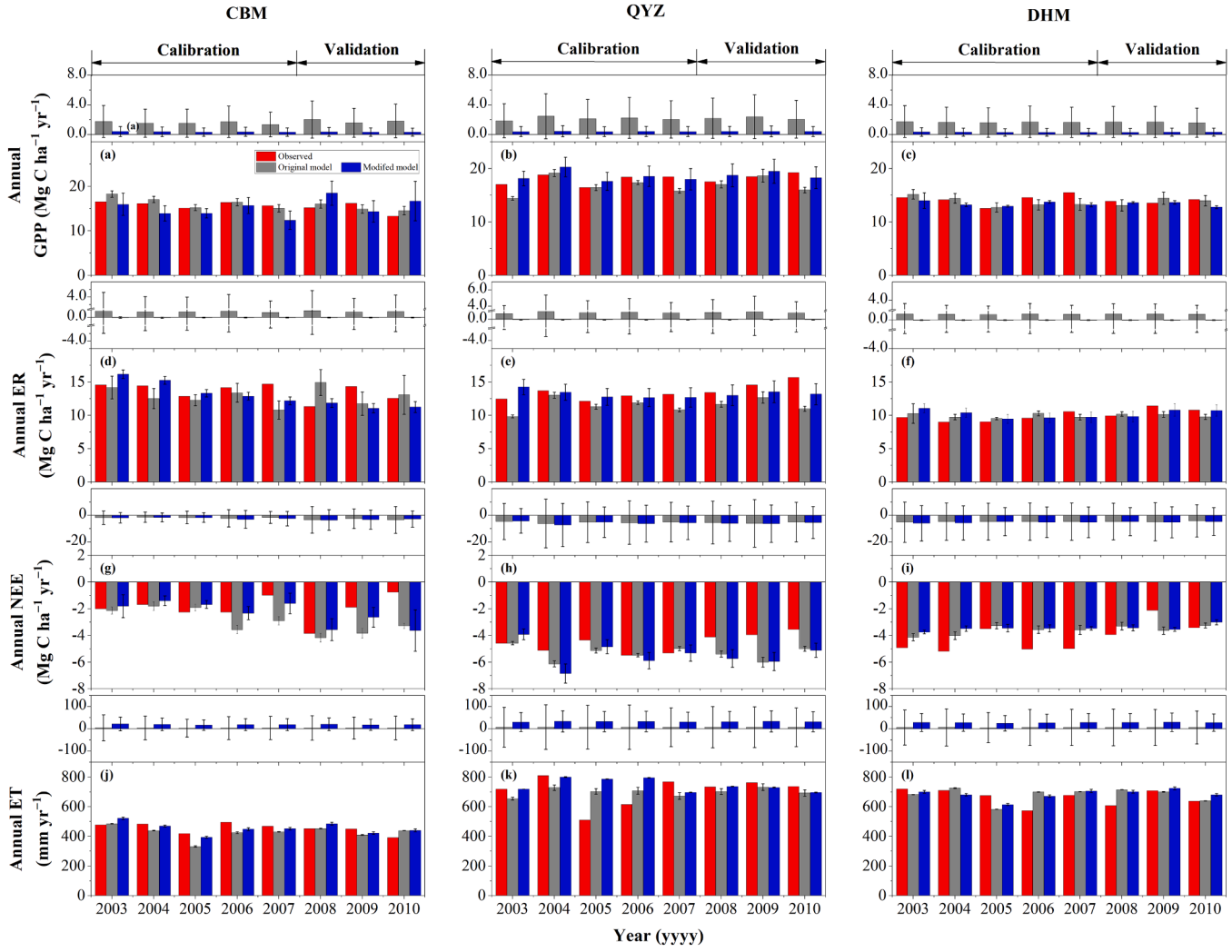

Fig. 3. Observed and simulated annual carbon fluxes of gross primary productivity (GPP), ecosystem respiration (ER) and net ecosystem-atmosphere exchange of carbon dioxide (NEE) and water vapour fluxes of evapotranspiration (ET) at three forest sites. The vertical bar crossing each datum point represents the uncertainty (95% confidence interval) induced by those of model inputs. Each box above panels represents total model error that was estimated by referring to the mean of model relative biases (MRBs) with vertical bars representing the uncertainties (95% confidence interval) estimated by referring to the double standard deviations of |MRBs|. The full site names of CBM, QYZ and DHM are referred to the footnotes of Table 1. The legends in panel a apply for all other panels. The simulations were provided by the original and modified CNMM-DNDC model.

improved NEE simulations for CBM in Taylor diagram (Fig. 2c), while its performance at QYZ and DHM remained comparable to the original model (Table S6). Evaluation statistics for NEE (NRMSE: 1.05–2.85; NSE: -0.11–0.47; R^2: 0.02–0.61; slope: 0.15–0.41) were generally poorer than for GPP and ER. Notably, the modified model corrected the unreasonable carbon uptake overestimations in spring at CBM of the original model (Fig. S1c). Despite differing GPP and ER performance, both models produced similar annual NEE estimates (Figs. 3g−i; Table S7). The modified model performed better for pure coniferous (QYZ) and mixed coniferous-deciduous (CBM) forests, showing particular strength in simulating GPP and ER dynamics across all sites, with NEE showing relatively weaker but still acceptable performance.

Daily ET dynamics were similar to GPP patterns due to closely coupling of transpiration with plant growth. While both models performed comparable well at CBM, the modified model showed significant improvements at QYZ and DHM where the original model failed to capture seasonal ET variations (Figs, S1d, S2d and S3d). Evaluation criteria for the simulated ET by the modified model showed NRMSE (0.32−0.46), NSE (0.59−0.81), R^2 (0.49−0.82) and slope (0.61−0.77) (Table S6), with Taylor diagram confirming substantial improvements at subtropical sites (Fig. 2d). Although extreme value compensation yielded similar annual ET estimates between models (Figs. 3j−l), the modified model better captured inter-annual variability (NSE > 0.60, Table S7), demonstrating enhanced capacity for simulating both daily and inter-annual ET dynamics across all forest types.

Statistical comparisons demonstrated significant improvements in the modified model's performance across all evaluated flux variables. When considering all variables ($n = 12$), the modified version reduced NRMSE by 38% ($p < 0.01$) and increased NSE from -0.26 to 0.54 and R^2 by 85% (0.39 to 0.72, $p < 0.05$). Excluding NEE ($n = 9$), these improvements were even more pronounced with 50% NRMSE reduction ($p < 0.01$), NSE increase from -0.34 to 0.68, and 90% R^2 enhancement (0.42 to 0.80, $p < 0.05$). These results highlight the obviously improved performances of the modified model in simulating daily carbon and water fluxes, particularly for GPP and ER dynamics.

3.2. Sensitivity of carbon fluxes to examined parameters or factors

The sensitivity analysis identified key eco-physiological parameters governing model performance across forest types. Both OAT and Morris methods identified canopy average specific leaf area (SLA, p30), fraction of leaf nitrogen in Rubisco (FLNR, p32), annual fraction of leaf and fine root turnover (LFRT, p6), and maximum stomatal conductance (g_{smax}, p33) as most influential for annual GPP and ER fluxes (Figs. 4-6). Parameters sensitivity exhibited distinct latitudinal patterns: FLNR dominated in temperate mixed forests (CBM), while LFRT became

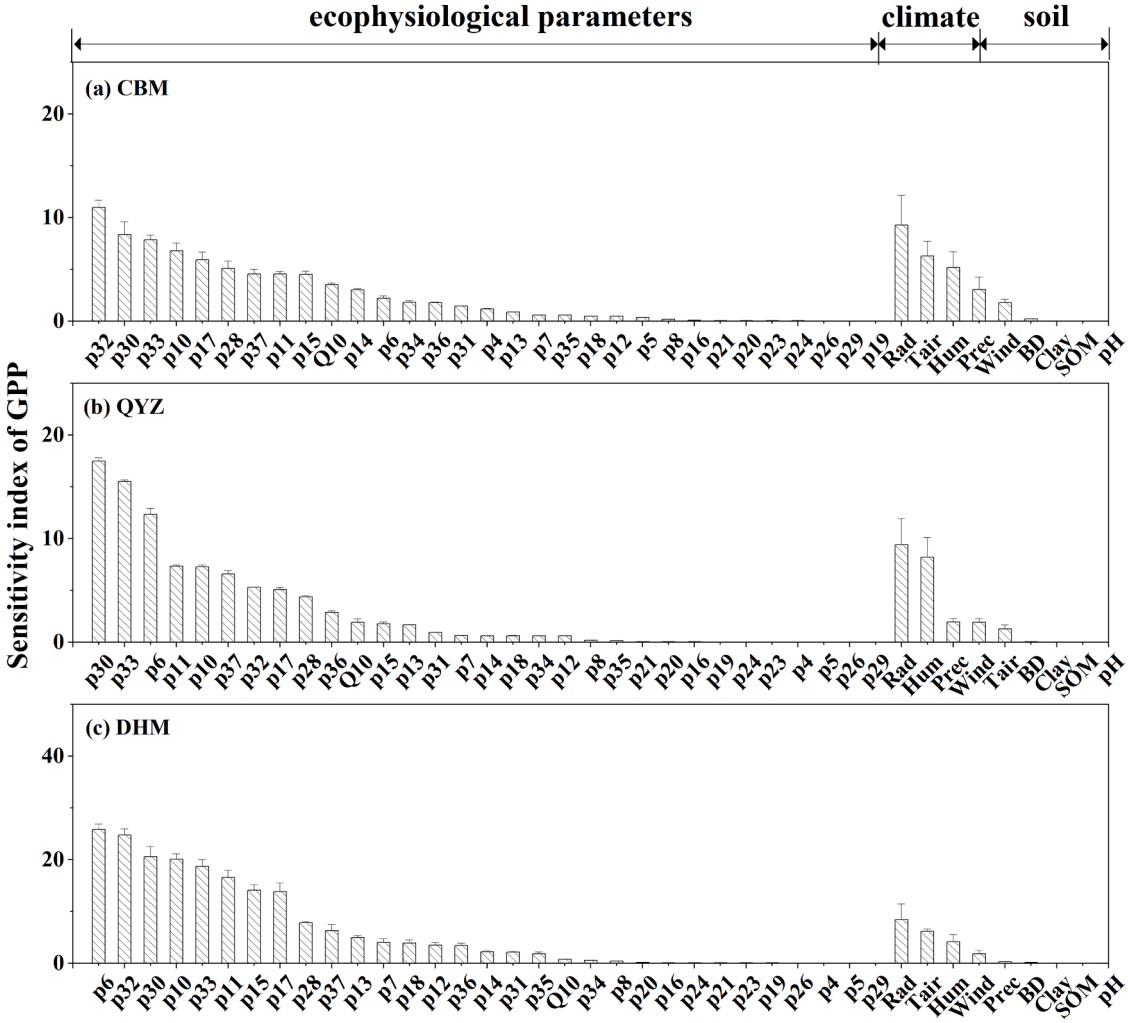

Fig. 4. Sensitivity indexes of modified CNMM-DNDC simulations on gross primary productivity (GPP) responding to alternations in individual eco-physiological parameters and model inputs of meteorological variables and soil properties at each site using the method of one-at-a-time. An index is given as the mean (a wide bar) and standard deviation (an error bar) of three indexes, each resulted from the simulations for one year. The parameter name and value for each parameter are referred to Table 1.

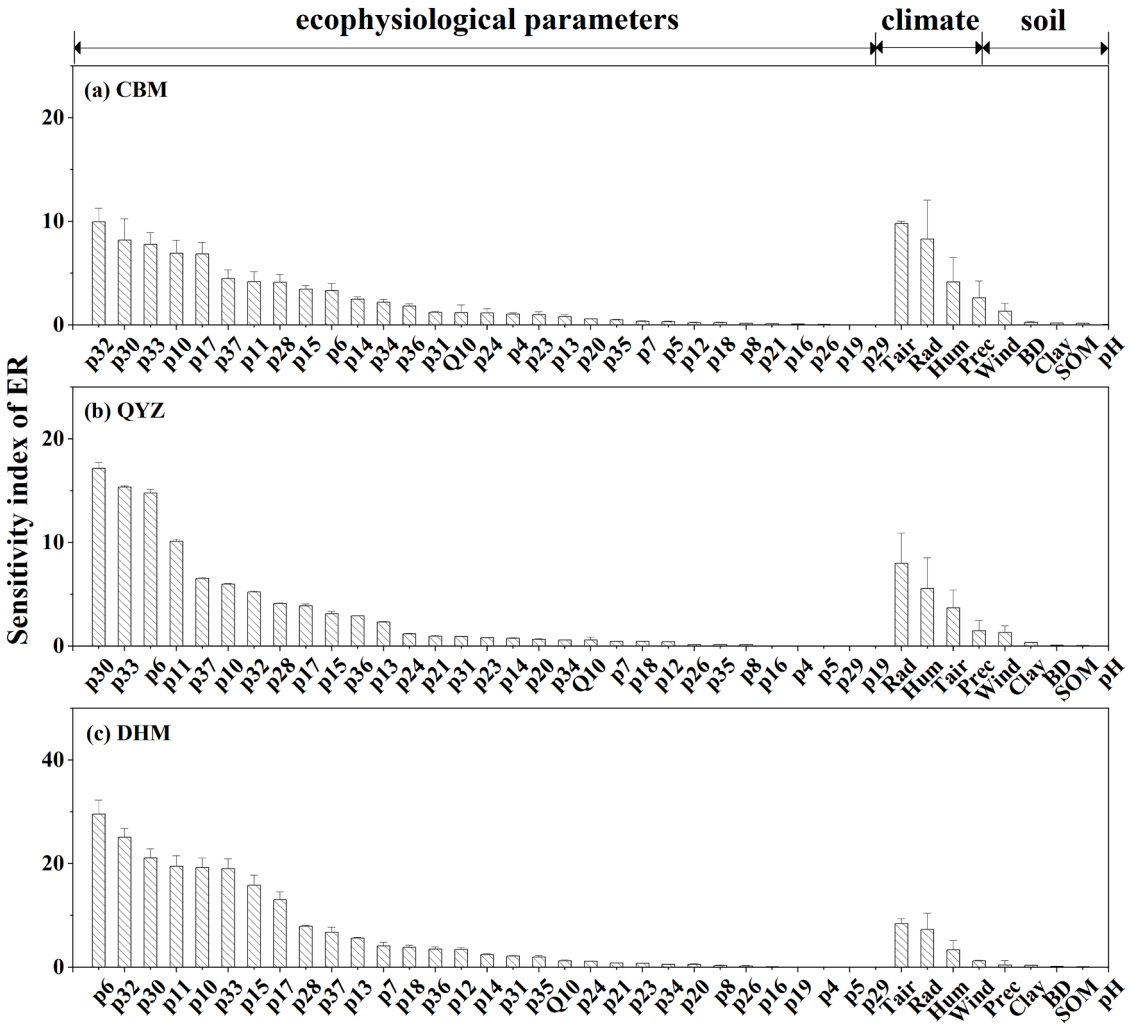

Fig. 5. Sensitivity indexes of modified CNMM-DNDC simulations on ecosystem respiration (ER) responding to alternations in individual eco-physiological parameters and model inputs of meteorological variables and soil properties at each site using the method of one-at-a-time. An index is given as the mean (a wide bar) and standard deviation (an error bar) of three indexes, each resulted from the simulations for one year. The parameter name and value for each parameter are referred to Table 1.

increasingly important in subtropical forests (QYZ, DHM), showing generally higher sensitivity index at lower latitudes (Figs. 4 and 5). While global sensitivity analysis largely confirmed OAT results at CBM (SLA, FLNR, carbon allocation rate of new fine root to new leaf (r_{frtol}, p10)) and QYZ (SLA, FLNR, LFRT), it uniquely identified light extinction coefficient (p28) as significant at DHM (Fig. 6). The analysis also revealed distinct vegetation-specific sensitivity patterns. While SLA predominantly governed ENT responses across all climate zones, FLNR emerged as the key driver for DBT in temperate regions and EBT in subtropical areas for GPP simulations (Fig S4). Evergreen needleleaf trees (ENT) exhibited strongest ER sensitivity to SLA, carbon and nitrogen ratios in fine roots (R_{frCN}, p17), LFRT and g_{smax}, while DBT and EBT showed primary responses to FLNR, LFRT and carbon to nitrogen ratios in leaves (R_{lCN}, p15) (Fig S5). These findings highlight how parameter sensitivity varies systematically with both forest composition and climate regime.

The sensitivity analysis showed that solar radiation exerted the strongest influence on carbon fluxes across all forest types, while other meteorological variables displayed site-specific effects. In mixed forests (CBM and DHM), both annual GPP and ER responded markedly to changes in solar radiation and air temperature, whereas the pure coniferous forest at QYZ showed greater sensitivity to solar radiation and humidity variations. These patterns were consistent for ENT across climatic zones, with GPP being particularly sensitive to solar radiation and humidity changes. In contrast, DBT and EBT demonstrated strongest responses to solar radiation and air temperature fluctuations (Figs. S4–S5). Global sensitivity analysis confirmed solar radiation as the dominant climatic driver while downplaying humidity and temperature effects (Fig. 6). Both methods consistently showed minimal sensitivity to soil properties (clay content, organic matter, pH, bulk density) across all forest types, with comparable sensitivity indices among sites.

4. Discussions

4.1. Model simulations on carbon fluxes

Forest GPP serves as a fundamental component of the terrestrial carbon pools across spatial scales, making its accurate estimation essential for understanding global carbon cycle (Campbell et al., 2017; Cook-Patton et al., 2020). Light use efficiency (LUE) models likes CASA and MODIS demonstrate strong capability in capturing spatiotemporal GPP patterns through utilization of extensive satellite observations (Potter et al., 1993; Running et al., 2004). A comprehensive evaluation of seven LUE models by Yuan et al. (2014) revealed their effectiveness in simulating daily GPP variations and magnitudes in deciduous broadleaf

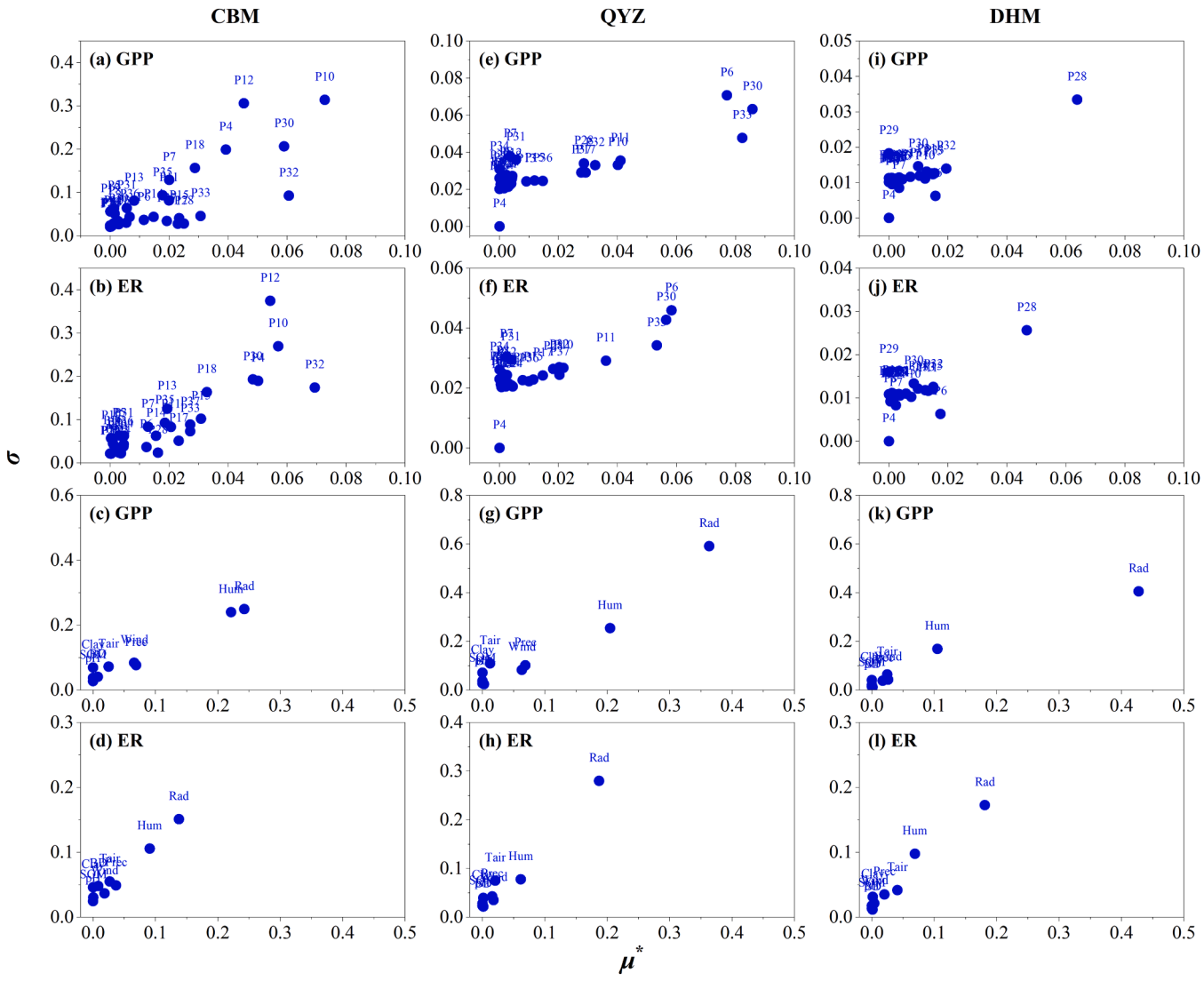

Fig. 6. The absolute average value (μ^*) and standard deviation (σ) of sensitivity analysis using Morris for the modified CNMM-DNDC simulations on gross primary productivity (GPP) and ecosystem respiration (ER) responding to alternations in eco-physiological parameters and model inputs of meteorological variables and soil properties at each site. The parameter name and value for each parameter are referred to Table 1.

and mixed forests (R^2 = 0.6–0.8). However, their predictive capacity remains constrained by reliance on historical satellite data (Yuan et al., 2014). In contrast, process-based models are specifically designed for future projections by mechanistically representing physical and biogeochemical processes (Srinet et al., 2023). Comparative studies in North America have shown that while both model types face challenges in reproducing inter-annual GPP variability, process-based models exhibit relatively better performance (R = 0.09–0.46) (Keenan et al., 2012; Raczka et al., 2013). The modified process-based model in this study demonstrated robust performance in simulating multi-year dynamics of daily GPP (R^2 = 0.5–0.9) and acceptable capability in capturing inter-annual variations (R^2 = 0.8), representing comparable or superior results to Biome-BGC implementations (Wen, 2019; Fan, 2021). The relatively poorer performance at DHM likely stems from difficulties in modelling photosynthesis of EBT, particularly in capturing subtle leaf phenology changes. These difficulties have been recognized in current models, which might be solved by incorporating new observational mechanisms and more comprehensive environmental regulation schemes for vegetation production (Raczka et al., 2013; Yuan et al., 2014). Furthermore, studies have shown that assimilating satellite data (e.g., LAI) can significantly enhance process-based models' ability to simulate spatial patters of daily GPP (Yan et al., 2016), suggesting a promising approach to improve modified CNMM-DNDC's performance across large spatial scales. Additionally, many studies have emphasized the global importance of leaf nitrogen and phosphorus co-limitation on photosynthetic capacity (Domingues et al., 2010; Walker et al., 2014), indicating that future model development should incorporate phosphorus limitation effects to achieve more comprehensive simulations.

Ecosystem respiration (ER), comprising both plant autotrophic and soil heterotrophic components, represents a critical carbon flux derived from organic matter decomposition across all ecosystem (Chapin et al., 2012). Accurate ER simulation is essential as its uncertainties can propagate errors to other carbon cycle variables like NEE and net primary production (Fang et al., 2022). While current terrestrial models often show poor performance in simulating annual soil respiration and its components (R^2 < 0.5, Lu et al., 2021), our modified model achieved substantially better multiple-year ER simulations across all sites (R^2 = 0.6), comparable to machine learning approaches (Lu et al., 2021). The pronounced growing-season ER differences between the CBM and DHM sites reflect well-documented latitudinal gradients in temperature and precipitation along North-South Transect in Eastern China (Yu et al., 2008). Field studies have documented substantial spatial variability in Q_{10} as a temperature sensitivity parameter of ER, which is usually a critical parameter in process-based models (Yu et al., 2008; Anav et al.,

2013). In updated growth module, Q_{10} affects maintenance respiration which not only was a component of ER but also affected photosynthesis directly. Sensitivity analysis revealed that simulated GPP exhibited greater responsiveness to Q_{10} variations than ER, as the latter incorporates additional contributions from growth respiration and heterotrophic soil respiration. The enhanced Q_{10} sensitivity at CBM with higher-latitude aligns with observational evidence (Yu et al., 2008; Zhang et al., 2019a), highlighting the importance of developing spatially explicit, mechanism-based parameterizations for Q_{10} to improve large-scale carbon budget estimations.

The modified model showed relatively poorer performance in simulating NEE compared to GPP and ER at both daily and annual scales, consistent with findings from other studies that attribute this challenge to error propagation from both GPP and ER components (Fang et al., 2022). Our daily NEE simulations (14.6−16.9 kg C ha^{-1} d^{-1}) demonstrated comparable accuracy to Biome-BGC model results (9.3−31.6 kg C ha^{-1} d^{-1}) reported by Liu et al. (2022b) for the same forest sites, whether using default parameters, calibrated parameters, or satellite-assimilated LAI data. At the annual scale, the consistently stronger correlation for GPP than NEE between simulations and observations reflects NEE's high sensitivity to minor relative errors in large GPP fluxes (Raczka et al., 2013). The weaker correlation for ER relative to GPP suggests that simulation errors of ER may be the primary limitation for capturing inter-annual variability of NEE. While process-based models like ours can effectively represent influences of temperature and soil moisture on carbon fluxes, both our results and previous studies (Keenan et al., 2012; Raczka et al., 2013) confirm these models still cannot fully explain observed inter-annual variability of NEE. These findings emphasize the importance of independently validating all carbon flux components to prevent error offsetting effects in ecosystem carbon budget assessments.

The eco-physiological parameters employed in this study are consistent with values reported in previous measurements or calibrations (Tables S8−S9; Li, 2018; Li, 2019; Fang, 2022). For the QYZ site, where local parameter measurements were limited, we adopted values from the DHM site except for the calibrated parameter. Notably, the FLNR parameter exhibited a latitudinal gradient, with increasing values toward higher latitudes that corresponds to the more vigorous growing season at CBM (Li, 2019). Li (2018) demonstrated significant spatial variability in key eco-physiological parameters for DBT and EBT, such as the carbon allocation rate of new fine root to new leaf (r_{frtol},p10), carbon allocation rate of new stem to new leaf (r_{stol}, p11) and vapour pressure deficit for the start of conductance reduction (p36). Our analysis confirms these parameters similarly exhibit latitudinal variation patterns, consistent with the reported spatial heterogeneity. While most parameters for QYZ and DHM originated from default values (Table 1), the model still achieved comparable performance across sites. This demonstrates the model's robustness when local parameterization data are limited, although incorporating site-specific parameters would certainly improve simulation accuracy.

The model incorporated user-defined mortality rates (White et al., 2000), despite growing evidence that stand-level mortality is regulated by complex interactions of stand characteristics (age, density, basal area, stand squared mean diameter at breast height), climate factors (standardized precipitation evapotranspiration index, drought length, mean annual temperature and precipitation), and topography (elevation, slope) (Subedi et al., 2021; Yan et al., 2024). Although advanced count-data models with random effects of survey plots have been developed for site-specific mortality estimation (Yan et al., 2024; Zhang et al., 2015b), process-based models still lack general parameterizations incorporating these multi-dimensional controls. Given mortality's substantial impact on forest productivity simulations (e.g. Aubry-Kientz et al., 2013; Bugmann et al., 2019), future development of process-based models should prioritize mechanistic representations of mortality responses to environmental gradients and disturbance regimes, building on existing frameworks for drought, carbon starvation, and wind damage (e.g. Johnson et al., 2016; McDowell et al., 2022).

4.2. Sensitivity analysis

4.2.1. Analysis of eco-physiological parameters

Plant autotrophic respiration accounts for nearly 50% of photosynthetically fixed carbon, establishing a strong positive correlation between GPP and ER in model simulations (Ryan, 1991; Piao et al., 2013; Jagermeyr et al., 2014). Our sensitivity analysis identified consistent parameter controls on both carbon fluxes, with SLA, FLNR, LFRT, g_{smax}, R_{lCN} and R_{frCN} emerging as dominant factors across all study sites. These findings align with previous researches (White et al., 2000; Raj et al., 2014; Miyauchi et al., 2019; Ren et al., 2022; Srinet et al., 2023).

Specific leaf area (SLA) emerged as a particularly influential parameter affecting both GPP and ER across all sites, with especially pronounced effects on ENT (Fig. S4). This prominent sensitivity reflects SLA's dual functional roles in: (1) determining LAI which fundamentally regulates canopy light capture efficiency, and (2) characterizing species positions along the leaf economic spectrum (White et al., 2000; Niinemets et al., 2015). Miyauchi et al. (2019) provided additional evidence for SLA's substantial impact on aboveground woody and leaf carbon density in *Eucommia ulmoides* plantations on the Loess Plateau. Given the marked variations in both GPP and ER induced by SLA differences (Srinet et al., 2023), potential model improvements could involve implementing differentiated SLA values for sun and shade leaves to better represent light gradient effects within forest canopies.

The parameter FLNR exhibited substantial influence on both GPP and ER, with particularly pronounced effects in broadleaf trees. This sensitivity stems from FLNR's fundamental regulation of the maximum carboxylation rate (V_{max}), since Rubisco serves as the primary enzyme catalysing atmospheric CO_2 assimilation (Stitt and Schulze, 1994; White et al., 2000). However, as emphasized by Houborg et al. (2012), V_{max} shows considerable spatial variability and remains challenging to quantify precisely, rendering FLNR a crucial yet uncertain parameter in process-based models. In addition, LFRT was identified as another sensitive parameter for forests in subtropical regions. For deciduous trees, where complete annual turnover of leaf and fine root carbon pools occurs (LFRT = 1.0), this contrasts with evergreen trees where LFRT shows an inverse relationship with mean leaf longevity (White et al., 2000). This distinction reflects the negative correlation between net photosynthetic capacity and leaf longevity reported by Reich et al. (1999), which represented through the positive relationship between LFRT and FLNR in our model.

Due to the pivotal role in mediating the balance between water loss and carbon assimilation (White et al., 2000; Miyauchi et al., 2019), g_{smax} was similarly recognized as a sensitive parameter. Recent theoretical advances in stomatal optimization (e.g. Medlyn et al., 2011; Lamour et al., 2022; Sabot et al., 2022), such as reconciliation of optimal and empirical approaches, offer promising approaches to refine stomatal conductance parameterization in future model updates. The R_{lCN} and R_{frCN} also exhibited notable sensitivity, particularly for DBT and the ENT in temperate region. In process-based models, e.g., the modified CNMM-DNDC, R_{lCN} determines nitrogen required for leaf construction and chlorophyll content, thereby affecting photosynthesis and leaf respiration (White et al., 2000; Ren et al., 2022). Although R_{frCN} has no direct influences on the uptakes of water and nutrients, it can control nitrogen requirement for fine root construction and nitrogen allocation to roots and shoots, and hence corresponding respirations (Raj et al., 2014).

Global analysis also confirmed the persistent importance of SLA, FLNR and LFRT across spatial scales. But effects of carbon allocation rate of new fine root to new leaf or canopy light extinction coefficient on annual GPP and ER could not be ignored at CBM or DHM, respectively. Canopy light extinction coefficient determines the amount of absorbed photosynthetically active radiation and thus regulates GPP and ER (White et al., 2000). These collective findings demonstrate that while

fundamental physiological mechanisms establish consistent parameter sensitivities, their relative importance varies substantially depending on species composition and environmental gradients (Raj et al., 2014), underscoring the necessity for meticulous parameterization in simulations.

4.2.2. Analysis of driving factors

The sensitivity analysis from both methods consistently identified solar radiation as the predominant meteorological driver of GPP variations. This is because solar radiation directly determines the rate of photosynthesis by regulating the amount of absorbed photosynthetically active radiation. Theoretically, enhanced solar radiation increases photosynthetic photon flux density, thereby stimulating photosynthetic activity (Yu et al., 2008). The impacts of solar radiation variations are particularly significant under cloudy conditions, when leaves typically operate below light saturation levels in contrast to full-sun scenarios (Yu et al., 2008). Our analysis revealed that even moderate increases in solar radiation during cloudy periods can substantially enhance vegetation productivity. This finding aligns with simulations from the BEPS and CLM-CN models, which are similarly reported radiation-induced GPP enhancements (Raczka et al., 2013).

Air temperature emerged as the secondary meteorological control in OAT analysis, but not Morris, primarily through its regulation of enzymatic activity for photosynthesis in mixed forests containing broadleaf species at both CBM and DHM sites (Farquhar et al., 1980). Temperature sensitivity of ER reflects its well-established dual dependence on both thermal regulation of metabolic processes and temperature-mediated plant productivity (Yu et al., 2008; Jagermeyr et al., 2014), a relationship confirmed in our sensitivity analysis. Both air temperature and solar radiation substantially influence ER dynamics by modulating enzymatic reaction rates and overall plant growth.

Humidity also demonstrated notable effects in both sensitivity methods. Elevated humidity reduces vapour pressure deficit, thereby enhancing leaf-scale stomatal conductance and consequently increasing GPP while decreasing ET (Sato et al., 2015). Interestingly, the minimal sensitivity to soil properties across both approaches suggests that observed spatial variations in GPP and ER in three sites primarily reflect latitudinal gradients in meteorological conditions rather than edaphic factors.

4.2.3. Analysis methods

Sensitivity analysis serves as a crucial methodology for quantifying the relative contributions of input parameters/variables to variations in model outputs, showing extensive applications in model calibration, diagnostic evaluation, and uncertainty assessment (Pianosi et al., 2016). In this study, we employed the one-at-a-time approach to systematically evaluate the impacts of newly incorporated eco-physiological parameters and model inputs on simulated GPP and ER fluxes in the modified CNMM-DNDC. However, the OAT method exhibits two fundamental limitations that warrant consideration. First, this approach can only assess the individual effect of a single parameter/input variable while holding all others constant, thereby precluding examination of potential interactions among multiple parameters. Second, the validity of OAT analysis becomes questionable when addressing non-linear relationships between target output variables and investigated parameters/input variables (Saltelli et al., 2008).

To address these methodological constraints, we complemented global sensitivity analysis using the Morris method, which enables comprehensive evaluation of parameter interactions and their collective influence on model outputs (Odongo et al., 2013; Raj et al., 2014). The observed discrepancies between two approaches across three study sites substantiate the recognized limitations of OAT method and underscore the necessity of implementing global sensitivity analysis that account for the integrated effects of multiple parameters/inputs (Saltelli et al., 2000; Odongo et al., 2013). These findings highlight the necessity of employing complementary sensitivity analysis approaches to obtain robust insights into model behaviour and parameter influences.

5. Conclusions

The Catchment Nutrient Management Model - DeNitrification-DeComposition (CNMM-DNDC) is a process-based hydro-biogeochemical model developed for simulating ecosystem processes relevant to the United Nations Sustainable Development Goals (SDGs) by 2030. However, the current version of this model uses the same simulation mechanism of plant growth for forest, grassland, wetland, and cropland vegetation, thus resulting in large biases in simulating dynamical carbon fluxes of forests. This study enhanced its forest carbon cycle representation by developing a specialized growth module referring to the Biome-BGC model. The modified processes included photosynthesis, allocation, respiration, mortality and litter decomposition. Evaluated against 8 years (2003–2010) of eddy covariance data from three Asian forest sites, the modified model showed significant improvements in simulating daily dynamics and annual variations of gross primary productivity (GPP), ecosystem respiration (ER) and evapotranspiration (ET), though net ecosystem carbon dioxide exchange (NEE) simulations remained challenging due to error compensation between GPP and ER. Sensitivity analysis revealed that carbon fluxes were most responsive to specific leaf area, fraction of leaf nitrogen in Rubisco and annual leaf and fine root turnover fraction among eco-physiological parameters, and to solar radiation, humidity and air temperature among meteorological drivers, while being insensitive to soil properties. The updated model was proven to be capable of estimating carbon fluxes of various forest ecosystems. It thus provides a potential tool for quantifying multiple ecosystem variables in close association with the SGDs, especially with improved credibility in simulating carbon fluxes and budgets of forests. However, the robust performances of the modified CNMM-DNDC in comprehensively simulating the aforementioned ecosystem variables for addressing multiple SDGs at different scales still need verification and confirmation in further studies.

CRediT authorship contribution statement

Wei Zhang: Writing – review & editing, Writing – original draft, Validation, Software, Methodology, Conceptualization. **Xunhua Zheng:** Writing – review & editing, Conceptualization. **Siqi Li:** Writing – review & editing, Validation. **Shenghui Han:** Writing – review & editing, Investigation. **Chunyan Liu:** Writing – review & editing, Investigation. **Zhisheng Yao:** Writing – review & editing, Investigation. **Rui Wang:** Writing – review & editing, Investigation. **Kai Wang:** Writing – review & editing, Investigation. **Xiao Chen:** Writing – review & editing, Investigation. **Guirui Yu:** Writing – review & editing, Data curation. **Zhi Chen:** Writing – review & editing, Data curation. **Jiabing Wu:** Writing – review & editing, Data curation. **Huimin Wang:** Writing – review & editing, Data curation. **Junhua Yan:** Writing – review & editing, Data curation. **Yong Li:** Writing – review & editing, Data curation.

Declaration of competing interest

The authors declare that they have no known competing financial interests or personal relationships that could have appeared to influence the work reported in this paper.

Acknowledgements

This study was jointly supported by the National Natural Science Foundation of China (U22A20562, 42330607), the National Key R&D Program of China (2022YFF0801904), the Chinese Academy of Sciences (XDA23070100, ZDBS-LY-DQC007), the National Large Scientific and Technological Infrastructure “Earth System Numerical Simulation Facility” (https://cstr.cn/31134.02.EL) and, S&T Program of Hebei (22373903D).

Supplementary materials

Supplementary material associated with this article can be found, in the online version, at doi:10.1016/j.ecolmodel.2025.111174.

Data availability

Data will be made available on request.

References

Anav, A., Friedlingstein, P., Kidston, M., Bopp, L., Ciais, P., Cox, P., Jones, C., Jung, M., Myneni, R., Zhu, Z., 2013. Evaluating the land and ocean components of the global carbon cycle in the CMIP5 earth system models. J. Climate 26, 6801–6843.

Aubry-Kientz, M., Herault, B., Ayotte-Trepanier, C., Baraloto, C., Rossi, V., 2013. Toward trait-based mortality models for tropical forests. PLoS. One 8.

Bond-Lamberty, B., Gower, S.T., Ahl, D.E., Thornton, P.E., 2005. Reimplementation of the Biome-BGC model to simulate successional change. Tree Physiol. 25, 413–424.

Bondeau, A., Smith, P.C., Zaehle, S., Schaphoff, S., Lucht, W., Cramer, W., Gerten, D., Lotze-Campen, H., MÜLler, C., Reichstein, M., Smith, B., 2007. Modelling the role of agriculture for the 20th century global terrestrial carbon balance. Global Change Biol. 13, 679–706.

Bugmann, H., Seidl, R., Hartig, F., Bohn, F., Bruna, J., Cailleret, M., et al., 2019. Tree mortality submodels drive simulated long-term forest dynamics: assessing 15 models from the stand to global scale, 10. Ecosphere, e02616.

Cai, Z., Yan, X., Gu, B., 2022. Applying C:N ratio to assess the rationality of estimates of carbon sequestration in terrestrial ecosystems and nitrogen budgets. Carbon Res. 1, 2.

Campbell, J.E., Berry, J.A., Seibt, U., Smith, S.J., Montzka, S.A., Launois, T., Belviso, S., Bopp, L., Laine, M., 2017. Large historical growth in global terrestrial gross primary production. Nature 544, 84–87.

Campolongo, F., Cariboni, J., Saltelli, A., 2007. An effective screening design for sensitivity analysis of large models. Environ. Modell. Softw. 22 (10), 1509–1518.

Chiesi, M., Maselli, F., Moriondo, M., Fibbi, L., Bindi, M., Running, S.W., 2007. Application of BIOME-BGC to simulate Mediterranean forest processes. Ecol. Model. 206, 179–190.

edited by Ciais, P., Sabine, C., Bala, G., Bopp, L., Brovkin, V., Canadell, J., Chhabra, A., DeFries, R., Galloway, J., Heimann, M., Jones, C., Le Quéré, C., Myneni, R.B., Piao, S., Thornton, P., 2013. Carbon and Other Biogeochemical Cycles, in: Climate Change 2013: The Physical Science Basis. In: Stocker, T.F., Qin, D., Plattner, G.K., Tignor, M., Allen, S.K., Boschung, J., Nauels, A., Xia, Y., Bex, V., Midgley, P.M. (Eds.), Contribution of Working Group I to the Fifth Assessment Report of the Intergovernmental Panel on Climate Change. Cambridge University Press, Cambridge, United Kingdom and New York, NY, USA. edited by.

Chapin, F.S., Matson, P.A., Vitousek, P.M., 2012. Principles of terrestrial ecosystem ecology.

Churkina, G., Brovkin, V., von Bloh, W., Trusilova, K., Jung, M., Dentener, F., 2009. Synergy of rising nitrogen depositions and atmospheric CO_2 on land carbon uptake moderately offsets global warming. Global Biogeochem. Cy. 23, GB4027.

Collatz, G.J., Ribas-Carbo, M., Berry, J.A., 1992. Coupled photosynthesis-stomatal conductance model for leaves of C_4 plants. Aust. J. Plant Physiol. 19, 519–538.

Congreves, K.A., Dutta, B., Grant, B.B., Smith, W.N., Desjardins, R.L., Wagner-Riddle, C., 2016. How does climate variability influence nitrogen loss in temperate agroecosystems under contrasting management systems? Agr. Ecosyst. Environ. 227, 33–41.

Cook-Patton, S.C., Leavitt, S.M., Gibbs, D., Harris, N.L., Lister, K., Anderson-Teixeira, K. J., Briggs, R.D., Chazdon, R.L., Crowther, T.W., Ellis, P.W., Griscom, H.P., Herrmann, V., Holl, K.D., Houghton, R.A., Larrosa, C., Lomax, G., Lucas, R., Madsen, P., Malhi, Y., Paquette, A., Parker, J.D., Paul, K., Routh, D., Roxburgh, S., Saatchi, S., van den Hoogen, J., Walker, W.S., Wheeler, C.E., Wood, S.A., Xu, L., Griscom, B.W., 2020. Mapping carbon accumulation potential from global natural forest regrowth. Nature 585, 545–550.

de Pury, D.G.G., Farquhar, G.D., 1997. Simple scaling of photosynthesis from leaves to canopies without the errors of big-leaf models. Plant Cell Environ. 20, 537–557.

Di Vittorio, A.V., Anderson, R.S., White, J.D., Miller, N.L., Running, S.W., 2010. Development and optimization of an Agro-BGC ecosystem model for C4 perennial grasses. Ecol. Model. 221, 2038–2053.

Domingues, T., Meir, P., Feldpausch, T., Saiz, G., Veenendaal, E., Schrodt, F., Bird, M., Djagbletey, G., Hien, F., Compaore, H., Diallo, A., Grace, J., Lloyd, J., 2010. Co-limitation of photosynthetic capacity by nitrogen and phosphorus in West Africa woodlands. Plant Cell Environ. 33, 959–980.

Dubache, G., Li, S., Zheng, X., Zhang, W., Deng, J., 2019. Modeling ammonia volatilization following urea application to winter cereal fields in the United Kingdom by improving a biogeochemical model. Sci. Total. Environ. 660, 1403–1418.

Fan, H., 2021. Simulation and analysis of water use efficiency in three terrestrial ecosystems. Northwest A & F Universit, y. Dissertation.

Fang, J., Shugart, H.H., Liu, F., Yan, X., Song, Y., Lv, F., 2022. FORCCHN V2.0: an individual-based model for predicting multiscale forest carbon dynamics. Geosci. Model. Dev. 15, 6863–6872.

Fang, M., 2022. Simulation of spatiotemporal dynamics of forest productivity in eastern China by Biome-BGC model and improvement of vegetation trait parameters. Beijing Forestry University. Dissertation.

FAO, 2020. Global Forest Resources Assessment 2020. FAO.

Farquhar, G., Caemmerer, S., Berry, J., 1980. A biochemical model of photosynthetic CO_2 assimilation in leaves of C_3 species. Planta 149, 78–90.

Fasman, G.D., 1976. Handbook of Biochemistry and Molecular Biology. Proteins, III. CRC Press, Cleveland, OH.

Friedlingstein, P., Prentice, I.C., 2010. Carbon–climate feedbacks: a review of model and observation based estimates. Curr. Opin. Env. Sust. 2, 251–257.

Gervois, S., de Noblet-Ducoudré, N., Viovy, N., Ciais, P., Brisson, N., Seguin, B., Perrier, A., 2004. Including croplands in a global biosphere model: methodology and evaluation at specific sites. Earth. Interact. 8, 1–25.

Guan, D., Wu, J., Zhao, X., Han, S., Yu, G., Sun, X., Jin, C.J., 2006. CO_2 fluxes over an old, temperate mixed forest in northeastern China. Agr. Forest Meteorol. 137, 138–149.

Haas, E., Klatt, S., Fröhlich, A., Kraft, P., Werner, C., Kiese, R., Grote, R., Breuer, L., Butterbach-Bahl, K., 2012. LandscapeDNDC: a process model for simulation of biosphere–atmosphere–hydrosphere exchange processes at site and regional scale. Landscape Ecol 28, 615–636.

Haxeltine, A., Prentice, I.C., 1996a. BIOME3: an equilibrium terrestrial biosphere model based on ecophysiological constraints, resource availability, and competition among plant functional types. Global Biogeochem. Cy. 10, 693–709.

Haxeltine, A., Prentice, I.C., 1996b. A general model for the light-use efficiency of primary production. Brit. Ecol. Soc. 10, 551–561.

Hidy, D., Barcza, Z., Haszpra, L., Churkina, G., Pintér, K., Nagy, Z., 2012. Development of the Biome-BGC model for simulation of managed herbaceous ecosystems. Ecol. Model. 226, 99–119.

Hidy, D., Barcza, Z., Marjanović, H., Ostrogović Sever, M.Z., Dobor, L., Gelybó, G., Fodor, N., Pintér, K., Churkina, G., Running, S., Thornton, P., Bellocchi, G., Haszpra, L., Horváth, F., Suyker, A., Nagy, Z., 2016. Terrestrial ecosystem process model Biome-BGCMuSo v4.0: summary of improvements and new modeling possibilities. Geosci. Model. Dev. 9, 4405–4437.

Houborg, R., Cescatti, A., Migliavacca, M., 2012. Constraining model simulations of GPP using satellite retrieved leaf chlorophyll. In: IEEE International Geoscience and Remote Sensing Symposium (IGARSS), pp. 6455–6458.

Jagermeyr, J., Gerten, D., Lucht, W., Hostert, P., Migliavacca, M., Nemani, R., 2014. A high-resolution approach to estimating ecosystem respiration at continental scales using operational satellite data. Global Change Biol. 20, 1191–1210.

Jia, Y., Wang, Q., Zhu, H., Chen, Z., He, N., Yu, G., 2019. A spatial and temporal dataset of atmospheric inorganic nitrogen wet depostion in China (1996-2015). China Science Data 4 (1). https://doi.org/10.11922/csdata.2018.0031.zh.

Jia, Y., Wang, Q., Zhu, H., Chen, Z., He, N., Yu, G., 2021. A spatial and temporal dataset of atmospheric inorganic nitrogen dry depostion in China (1996-2015). China Science Data 6 (2). https://doi.org/10.11922/csdata.2019.0078.zh.

Johnson, M.O., Galbraith, D., Gloor, M., De Deurwaerder, H., Guimberteau, M., Rammig, A., et al., 2016. Variation in stem mortality rates determines patterns of above-ground biomass in Amazonian forests: implications for dynamic global vegetation models. Global Change Biol 22, 3996–4013.

Jones, H.G., 1992. Plants and Microclimate. Cambridge University Press, Cambridge.

Keenan, T.F., Baker, I., Barr, A., Ciais, P., Davis, K., Dietze, M., Dragoni, D., Gough, C.M., Grant, R., Hollinger, D., Hufkens, K., Poulter, B., McCaughey, H., Raczka, B., Ryu, Y., Schaefer, K., Tian, H., Verbeeck, H., Zhao, M., Richardson, A.D., 2012. Terrestrial biosphere model performance for inter-annual variability of land-atmosphere CO_2 exchange. Global Change Biol. 18, 1971–1987.

Krinner, G., Viovy, N., de Noblet-Ducoudré, N., Ogée, J., Polcher, J., Friedlingstein, P., Ciais, P., Sitch, S., Prentice, I.C., 2005. A dynamic global vegetation model for studies of the coupled atmosphere-biosphere system. Global Biogeochem. Cy. 19, GB1015.

Lamour, J., Davidson, K.J., Ely, K.S., Le Moguédec, G., Leakey, A.D.B., Li, Q., Serbin, S., Rogers, A., 2022. An improved representation of the relationship between photosynthesis and stomatal conductance leads to more stable estimation of conductance parameters and improves the goodness-of-fit across diverse data sets. Global Change Biol. 28, 3537–3556.

Li, C., 2007. Quantifying greenhouse gas emissions from soils: Scientific basis and modeling approach. Soil Sci. Plant Nutr. 53, 344–352.

Li, C., Frolking, S., Frolking, T.A., 1992. A model of nitrous oxide evolution from soil driven by rainfall events: 1. Model structure and sensitivity. J. Geophys. Res. 97, 9759–9776.

Li, S., Zhang, W., Zheng, X., Li, Y., Han, S., Wang, R., Wang, K., Yao, Z., Liu, C., Zhang, C., 2022. Update of a biogeochemical model with process-based algorithms to predict ammonia volatilization from fertilized cultivated uplands and rice paddy fields. Biogeosciences. 19, 3001–3019.

Li, S., Zheng, X., Zhang, W., Han, S., Deng, J., Wang, K., Wang, R., Yao, Z., Liu, C., 2019. Modeling ammonia volatilization following the application of synthetic fertilizers to cultivated uplands with calcareous soils using an improved DNDC biogeochemistry model. Sci. Total. Environ. 660, 931–946.

Li, S., Zhu, B., Zheng, X., Hu, P., Han, S., Fan, J., Wang, T., Wang, R., Wang, K., Yao, Z., Liu, C., Zhang, W., Li, Y., 2023. Enabling a process-oriented hydro-biogeochemical model to simulate soil erosion and nutrient losses. Biogeosciences. 20, 3555–3572.

Li, X., 2019. Study on the relationship between vegetation productivity and water use in broadleaved-Korean pine forest zone of Changbai Mountain of Jilin province. Beijing Forestry University, Northeast China. Dissertation.

Li, Y., Shen, J., Wang, Y., Gao, M., Liu, F., Zhou, P., Liu, X., Chen, D., Zou, G., Luo, Q., Ma, Q., 2017. CNMM: a grid-based spatially-distributed catchment simulation model. China Science Press, Beijing (in Chinese).

Li, Y., 2018. Spatiotemporal heterogeneity analysis of parameter sensitivity of ecological process model—the BIOME-BGC model as an example. Northwest A & F University. Dissertation.

Liang, H., Hu, K., Batchelor, W.D., Qi, Z., Li, B., 2016. An integrated soil-crop system model for water and nitrogen management in North China. Sci. Rep. 6, 25755.
Liu, K., Ran, Q., Li, F., Shaheen, S.M., Wang, H., Rinklebe, J., Liu, C., Fang, L., 2022a. Carbon-based strategy enables sustainable remediation of paddy soils in harmony with carbon neutrality. Carbon Res. 1, 12.
Liu, Q., Zhang, T., Du, M., Gao, H., Zhang, Q., Sun, R., 2022b. A better carbon-water flux simulation in multiple vegetation types by data assimilation. For. Ecosyst. 9, 100013.
Lu, H., Li, S., Ma, M., Bastrikov, V., Chen, X., Ciais, P., Dai, Y., Ito, A., Ju, W., Lienert, S., Lombardozzi, D., Lu, X., Maignan, F., Nakhavali, M., Quine, T., Schindlbacher, A., Wang, J., Wang, Y., Wårlind, D., Zhang, S., Yuan, W., 2021. Comparing machine learning-derived global estimates of soil respiration and its components with those from terrestrial ecosystem models. Environ. Res. Lett. 16, 054048.
Majkowski, J., Ridgeway, J.M., Miller, D.R., 1981. Multiplicative sensitivity analysis and its role in development of simualtion models. Ecol. Model. 12, 191–208.
Makela, A., Landsberg, J., Ek, A.R., Burk, T.E., Ter-Mikaelian, M., Ågren, G.I., Oliver, C. D., Puttonen, P., 2000. Process-based models for forest ecosystem management: current state of the art and challenges for practical implementation. Tree Physiol. 20, 289–298.
Mao, F., Li, P., Zhou, G., Du, H., Xu, X., Shi, Y., Mo, L., Zhou, Y., Tu, G., 2016. Development of the BIOME-BGC model for the simulation of managed Moso bamboo forest ecosystems. J. Environ. Manage 172, 29–39.
McDowell, N.G., Sapes, G., Pivovaroff, A., Adams, H.D., Allen, C.D., Anderegg, W.R.L., et al., 2022. Mechanisms of woody-plant mortality under rising drought, CO_2 and vapour pressure deficit. Nat. Rev. Earth. Environ. 1–15.
Medlyn, B.E., Duursma, R.A., Eamus, D., Ellsworth, D.S., Prentice, I.C., Barton, C.V.M., Crous, K., Angelis, P., Freeman, M., Wingate, L., 2011. Reconciling the optimal and empirical approaches to modelling stomatal conductance. Global Change Biol. 17, 2134–2144.
Miyauchi, T., Machimura, T., Saito, M., 2019. Estimating carbon fixation of plant organs for afforestation monitoring using a process-based ecosystem model and ecophysiological parameter optimization. Ecol. Evol. 9, 8025–8041.
Moriasi, D., Arnold, J., Van Liew, M., Bingner, R., Harmel, R., Veith, T., 2007. Model evaluation guidelines for systematic quantification of accuracy in watershed simulation. T. Am. Soc. Agr. Biol. Eng. 50, 885–900.
Morris, M.D., 1991. Factorial sampling plans for preliminary computational experiments. Technometrics. 33, 161–174.
Nash, J., Sutcliffe, J., 1970. River flow forecasting through conceptual models: part I- a discussion of principles. J. Hydrol. 10, 282–290.
Niinemets, Ü., Keenan, T.F., Hallik, L., 2015. A worldwide analysis of within-canopy variations in leaf structural, chemical and physiological traits across plant functional types. New. Phytol. 205, 973–993.
Nobel, P.S., 1991. Phsiochemical and Environmental Plant Physiology. Academic Press, San Diego, CA.
Odongo, V.O., Onyando, J.O., Mutua, B.M., van Oel, P.R., Becht, R., 2013. Sensitivity analysis and calibration of the Modified Universal Soil Loss Equation (MUSLE) for the upper Malewa Catchment. Kenya. Int. J. Sediment Res. 28, 368–383.
Palosuo, T., Foereid, B., Svensson, M., Shurpali, N., Lehtonen, A., Herbst, M., Linkosalo, T., Ortiz, C., Rampazzo Todorovic, G., Marcinkonis, S., Li, C., Jandl, R., 2012. A multi-model comparison of soil carbon assessment of a coniferous forest stand. Environ. Modell. Softw. 35, 38–49.
Pianosi, F., Beven, K., Freer, J., Hall, J.W., Rougier, J., Stephenson, D.B., Wagener, T., 2016. Sensitivity analysis of environmental models: A systematic review with practical workflow. Environ. Modell. Softw. 79, 214–232.
Piao, S., Sitch, S., Ciais, P., Friedlingstein, P., Peylin, P., Wang, X., Ahlstrom, A., Anav, A., Canadell, J.G., Cong, N., Huntingford, C., Jung, M., Levis, S., Levy, P.E., Li, J., Lin, X., Lomas, M.R., Lu, M., Luo, Y., Ma, Y., Myneni, R.B., Poulter, B., Sun, Z., Wang, T., Viovy, N., Zaehle, S., Zeng, N., 2013. Evaluation of terrestrial carbon cycle models for their response to climate variability and to CO2 trends. Global Chang Biol. 19, 2117–2132.
Potter, C.S., Randerson, J.T., Field, C.B., Matson, P.A., Vitousek, P.M., Mooney, H.A., 1993. Terrestrial ecosystem production: a process model based on global satellite and surface data. Global Biogeochem. Cy. 74, 811–841.
Raczka, B.M., Davis, K.J., Huntzinger, D., Neilson, R.P., Poulter, B., Richardson, A.D., Xiao, J., Baker, I., Ciais, P., Keenan, T.F., Law, B., Post, W.M., Ricciuto, D., Schaefer, K., Tian, H., Tomelleri, E., Verbeeck, H., Viovy, N., 2013. Evaluation of continental carbon cycle simulations with North American flux tower observations. Ecol. Monogr. 83, 531–556.
Raj, R., Hamm, N.A.S., van der Tol, C., Stein, A., 2014. Variance-based sensitivity analysis of BIOME-BGC for gross and net primary production. Ecol. Model. 292, 26–36.
Reich, P.B., Ellsworth, D.S., Walters, M.B., Vose, J.M., Gresham, C., Volin, J.C., Bowman, W.D., 1999. Generality of leaf trait relationships: a test across six biomes. Ecology. 80, 1955–1969.
Ren, H., Zhang, L., Yan, M., Tian, X., Zheng, X., 2022. Sensitivity analysis of Biome-BGCMuSo for gross and net primary productivity of typical forests in China. For. Ecosyst. 9, 100011.
Running, S.W., Nemani, R.R., Heinsch, F.A., Zhao, M., Reeves, M., Hashimoto, H., 2004. A continuous satellite-derived measure of global terrestrial primary production. Bioscience 54, 547–560.
Ryan, M.G., 1991. Effects of climate change on plant respiration. Ecol. Appl. 1, 157–167.
Sabot, M.E.B., De Kauwe, M.G., Pitman, A.J., Medlyn, B.E., Ellsworth, D.S., Martin-StPaul, N.K., Wu, J., Choat, B., Limousin, J., Mitchell, P., Rogers, A., Serbin, S., 2022. One stomatal model to rule them all? toward improved representation of carbon and water exchange in global models. J. Adv. Model. Earth. Syst. 14, e2021MS002761.
Saltelli, A., Chan, K., Scott, E.M., 2000. SensitivityAnalysis. Wiley, Chichester.
Saltelli, A., Ratto, M., Andres, T., Campolongo, F., Cariboni, J., Gatelli, D., Saisana, M., Tarantola, S., 2008. Global Sensitivity Analysis: The Primer. John Wiley & Sons, Ltd., Chichester.
Sato, H., Kumagai, T.o., Takahashi, A., Katul, G.G., 2015. Effects of different representations of stomatal conductance response to humidity across the African continent under warmer CO_2-enriched climate conditions. J. Geophys. Res–Biogeo. 120, 979–988.
Schulze, E.D., Luyssaert, S., Ciais, P., Freibauer, A., Janssens, I.A., Soussana, J.F., Smith, P., Grace, J., Levin, I., Thiruchittampalam, B., Heimann, M., Dolman, A.J., Valentini, R., Bousquet, P., Peylin, P., Peters, W., Rödenbeck, C., Etiope, G., Vuichard, N., Wattenbach, M., Nabuurs, G.J., Poussi, Z., Nieschulze, J., Gash, J.H., Team, C., 2009. Importance of methane and nitrous oxide for Europe's terrestrial greenhouse-gas balance. Nat. Geosic. 2, 842–850.
Seidl, R., Thom, D., Kautz, M., Martin-Benito, D., Peltoniemi, M., Vacchiano, G., Wild, J., Ascoli, D., Petr, M., Honkaniemi, J., Lexer, M.J., Trotsiuk, V., Mairota, P., Svoboda, M., Fabrika, M., Nagel, T.A., Reyer, C.P.O., 2017. Forest disturbances under climate change. Nat. Clim. Change 7, 395–402.
Sitch, S., Smith, B., Prentice, I.C., Arneth, A., Bondeau, A., Cramer, W., Kaplan, J.O., Levis, S., Lucht, W., Sykes, M.T., Thonicke, K., Venevsky, S., 2003. Evaluation of ecosystem dynamics, plant geography and terrestrial carbon cycling in the LPJ dynamic global vegetation model. Global Change Biol. 9, 161–185.
Srinet, R., Nandy, S., Patel, N.R., Padalia, H., Watham, T., Singh, S.K., Chauhan, P., 2023. Simulation of forest carbon fluxes by integrating remote sensing data into biome-BGC model. Ecol. Model. 475, 110185.
Stitt, M., Schulze, D., 1994. Does Rubisco control the rate of photosynthesis and plant growth? An exercise in molecular ecophysiology. Plant Cell Environ. 17, 465–487.
Subedi, M., Xi, W., Edgar, C., Rideout-Hanzak, S., Yan, M., 2021. Tree mortality and biomass loss in drought-affected forests of East Texas. USA. J. Forestry Res. 32, 67–80.
Tatarinov, F.A., Cienciala, E., 2006. Application of BIOME-BGC model to managed forests. Forest Ecol. Manag. 237, 267–279.
Thomas, R.Q., Bonan, G.B., Goodale, C.L., 2013. Insights into mechanisms governing forest carbon response to nitrogen deposition: a model–data comparison using observed responses to nitrogen addition. Biogeosciences 10, 3869–3887.
Thornton, P., Law, B., Gholz, H.L., Clark, K.L., Falge, E., Ellsworth, D., Goldstein, A., Monson, R., Hollinger, D., Falk, M., Chen, J., Sparks, J., 2002. Modeling and measuring the effects of disturbance history and climate on carbon and water budgets in evergreen needleleaf forests. Agr. Forest Meteorol. 113, 185–222.
Thornton, P.E., Lamarque, J.F., Rosenbloom, N.A., Mahowald, N.M., 2007. Influence of carbon-nitrogen cycle coupling on land model response to CO_2 fertilization and climate variability. Global Biogeochem. Cy. 21, GB4018.
Thornton, P.E., Rosenbloom, N.A., 2005. Ecosystem model spin-up: Estimating steady state conditions in a coupled terrestrial carbon and nitrogen cycly model. Ecol. Model. 189, 25–48.
Walker, A., Beckerman, A., Gu, L., Kattge, J., Cernusak, L.A., Domingues, T., Scales, J., Wohlfahrt, G., Wullschleger, S., Woodward, F., 2014. The relationship of leaf photosynthetic traits-V_{cmax} and J_{max}-to leaf nitrogen, leaf phosphorus, and specific leaf area: a meta-analysis and modeling study. Ecol. Evol. 4 (16), 3218–3235.
Wang, W., Ichii, K., Hashimoto, H., Michaelis, A.R., Thornton, P.E., Law, B.E., Nemani, R. R., 2009. A hierarchical analysis of terrestrial ecosystem model Biome-BGC: equilibrium analysis and model calibration. Ecol. Model. 220, 2009–2023.
Waring, R.H., Pitman, G.B., 1985. Modifying lodgepole pine stands to change susceptibility to mountain pine beetle attack. Ecology 66, 889–897.
Waring, R.H., Running, S.W., 2007. Forest Ecosystems: Analysis at Multiple Scales. Elsevier Academic Press, Francisco, CA.
Wen, Y., 2019. Coupling of landscape pattern and water use efficiency based on Biome-BGC model. Beijing Forestry University. Dissertation.
White, M.A., Thornton, P.E., Running, S.W., Nemani, R.R., 2000. Parameterization and sensitivity analysis of the Biome-BGC terrestrial ecosystem model: net primary production controls. Earth. Interact. 4, 1–85.
Wigmosta, M., Vail, L., Lettenmaier, D., 1994. A distributed hydrology-vegetation model for complex terrain. Water. Resour. Res. 30, 1665–1679.
Willmott, C., Matsuurra, K., 2005. Advantages of the mean aboslute error (MAE) over the root mean square error (RMSE) in assessing average model performance. Clim. Res. 30, 79–82.
Woodrow, I.E., Berry, J.A., 1988. Enzymatic regulation of photosynthetic CO_2 fixation in C_3 plants. Annu. Rev. Plant Physiol. Plant Molecular Biol. 39, 533–594.
Wu, L., McGechan, M.B., McRoberts, N., Baddeley, J.A., Watson, C.A., 2007. SPACSYS: Integration of a 3D root architecture component to carbon, nitrogen and water cycling—model description. Ecol. Model. 200, 343–359.
Wu, Y., Liu, S., Qiu, L., Sun, Y., 2016. SWAT-DayCent coupler: an integration tool for simultaneous hydro-biogeochemical modeling using SWAT and DayCent. Environ. Modell. Softw. 86, 81–90.
Yan, M., Chen, Y., Yan, J., Xi, W., 2024. Studing forest tree mortality based on a generalized linear mixed-effects model. Acta Ecologicca Sinica 44, 2420–2436.
Yan, M., Tian, X., Li, Z., Chen, E., Wang, X., Han, Z., Sun, H., 2016. Simulation of forest carbon fluxes using model incorporation and data assimilation. Remote Sens 8, 567.
Yu, G., Zhang, L., Sun, X., Fu, Y., Wen, X., Wang, Q., Li, S., Ren, C., Song, X., Liu, Y., Han, S., Yan, J., 2008. Environmental controls over carbon exchange of three forest ecosystems in eastern China. Global Change Biol. 14, 2555–2571.
Yu, G., Zhu, X., Fu, Y., He, H., Wang, Q., Wen, X., Li, X., Zhang, L., Zhang, L., Su, W., Li, S., Sun, X., Zhang, Y., Zhang, J., Yan, J., Wang, H., Zhou, G., Jia, B., Xiang, W., Li, Y., Zhao, L., Wang, Y., Shi, P., Chen, S., Xin, X., Zhao, F., Wang, Y., Tong, C., 2013. Spatial patterns and climate drivers of carbon fluxes in terrestrial ecosystems of China. Global Change Biol. 19, 798–810.

Yuan, W., Cai, W., Xia, J., Chen, J., Liu, S., Dong, W., Merbold, L., Law, B., Arain, A., Beringer, J., Bernhofer, C., Black, A., Blanken, P.D., Cescatti, A., Chen, Y., Francois, L., Gianelle, D., Janssens, I.A., Jung, M., Kato, T., Kiely, G., Liu, D., Marcolla, B., Montagnani, L., Raschi, A., Roupsard, O., Varlagin, A., Wohlfahrt, G., 2014. Global comparison of light use efficiency models for simulating terrestrial vegetation gross primary production based on the LaThuile database. Agr. Forest Meteorol. 192–193, 108–120.

Zeng, H., Liu, Q., Feng, Z., Wang, X., Ma, Z., 2008. GPP and NPP study of *Pinus elliottii* forest in red soil hilly region based on BIOME-BGC model. Acta Ecol. Sinica 28, 5314–5321.

Zhang, L., Luo, Y., Liu, M., Chen, Z., Su, W., He, H., Zhu, Z., Sun, X., Wang, Y., Zhou, G., Zhao, X., Han, S., Ouyang, Z., Zhang, X., Zhang, Y., Liu, Q., Hao, Y., Yan, J., Zhang, D., Li, Y., Wang, A., Wu, J., Li, F., Zhao, F., Shi, P., Zhang, Y., He, Y., Lin, L., Song, Q., Wang, H., Liu, Y., Yu, G., 2019a. Carbon and water fluxes observed by the Chinese flux observation and research network (2003–2005). China Sci. Data 4, 2018-2012-2029.

Zhang, W., Li, S., Han, S., Zheng, X., Xie, H., Lu, C., Sui, Y., Wang, R., Liu, C., Yao, Z., Li, T., 2021a. Less intensive nitrate leaching from Phaeozems cultivated with maize generally occurs in northeastern China. Agr. Ecosyst. Environ. 310, 107303.

Zhang, W., Li, Y., Li, S., Zheng, X., 2024. The CNMM-DNDC V6.0 with the updates for simulating dynamical forest-atmosphere exchanges of carbon and evapotranspiration. Zenodo. https://doi.org/10.5281/zenodo.13363688.

Zhang, W., Li, Y., Zhu, B., Zheng, X., Liu, C., Tang, J., Su, F., Zhang, C., Ju, X., Deng, J., 2018. A process-oriented hydro-biogeochemical model enabling simulation of gaseous carbon and nitrogen emissions and hydrologic nitrogen losses from a subtropical catchment. Sci. Total. Environ. 616–617, 305–317.

Zhang, W., Liu, C., Zheng, X., Wang, K., Cui, F., Wang, R., Li, S., Yao, Z., Zhu, J., 2019b. Using a modified DNDC biogeochemical model to optimize field management of a multi-crop (cotton, wheat, and maize) system: a site-scale case study in northern China. Biogeosciences 16, 2905–2922.

Zhang, W., Liu, C., Zheng, X., Zhou, Z., Cui, F., Zhu, B., Haas, E., Klatt, S., Butterbach-Bahl, K., Kiese, R., 2015a. Comparison of the DNDC, LandscapeDNDC and IAP-N-GAS models for simulating nitrous oxide and nitric oxide emissions from the winter wheat–summer maize rotation system. Agr. Syst. 140, 1–10.

Zhang, W., Yao, Z., Li, S., Zheng, X., Zhang, H., Ma, L., Wang, K., Wang, R., Liu, C., Han, S., Deng, J., Li, Y., 2021b. An improved process-oriented hydro-biogeochemical model for simulating dynamic fluxes of methane and nitrous oxide in alpine ecosystems with seasonally frozen soils. Biogeosciences. 18, 4211–4225.

Zhang, W., Yao, Z., Zheng, X., Liu, C., Wang, R., Wang, K., Li, S., Han, S., Zuo, Q., Shi, J., 2020. Effects of fertilization and stand age on N_2O and NO emissions from tea plantations: a site-scale study in a subtropical region using a modified biogeochemical model. Atmos. Chem. Phys. 20, 6903–6919.

Zhang, X., Lei, Y., Liu, X., 2015b. Modeling stand mortality using Poisson mixture models with mix-effects. IForest 8, 333–338.

Zhou, G., Peng, C., Li, Y., Liu, S., Zhang, Q., Tang, X., Liu, J., Yan, J., Zhang, D., Chu, G., 2013. A climate change-induced threat to the ecological resilience of a subtropical monsoon evergreen broad-leaved forest in Southern China. Global Change Biol. 19, 1197–1210.